2015-07-01

Temperature Measurement Using Infrared Spectral Band Emissions From H2O

Daniel Jared Ellis
Brigham Young University - Provo

Temperature Measurement Using Infrared Spectral Band Emissions From H_2O

Daniel Jared Ellis

A thesis submitted to the faculty of
Brigham Young University
in partial fulfillment of the requirements for the degree of

Master of Science

Dale R. Tree, Chair
Julie Crockett
Brian D. Iverson

Department of Mechanical Engineering

Brigham Young University

July 2015

ABSTRACT

Temperature Measurement Using Infrared Spectral Band Emissions From H_2O

Daniel Jared Ellis
Department of Mechanical Engineering, BYU
Master of Science

Currently there is no known method for accurately measuring the temperature of the gas phase of combustion products within a solid fuel flame. The industry standard is a suction pyrometer and thermocouple which is intrusive, both spatially and temporally averaging, and difficult to use. In this work a new method utilizing the spectral emission from water vapor is investigated through modeling and experimental measurements. This method was demonstrated along a 0.75m line of sight, averaged over 1 minute in the products of a natural gas flame but has the potential to produce a spatial resolution on the order of 5 cm and a temporal resolution of less than 1 millisecond. The method employs the collection of infrared emission from water vapor over discrete wavelength bands and then uses the ratio of those emissions to infer temperature. A 12.5 mm lens has been positioned within a water cooled probe to focus flame product gas emission into an optical fiber where the light is transmitted to a Fourier Transform Infrared Spectrometer (FTIR). The same optical setup was also used to collect light from a black body cavity at a known temperature in order to calibrate the spectral sensitivity of the optical system and FTIR detector. Experiments were conducted in the product gas of a 150 kW_{th} methane flame comparing the optical emission results to a suction pyrometer with type K thermocouple. The optical measurement produced gas temperatures approximately 1 - 4% higher than the suction pyrometer. Broadband background emission was also seen by the optical measurement and was removed assuming grey body radiation. This background emission can be used to determine particle emission temperature and intensity. Additional work will be needed to demonstrate the method under conditions with significant particle emission. Additional work is also needed to demonstrate the work over a smaller path length and shorter time scale.

Keywords: infrared, spectral, temperature, H_2O, FTIR

ACKNOWLEDGEMENTS

I would like to acknowledge help from many different sources. Above all, I acknowledge the help I have received from Heavenly Father during the course of this project. Secondly I would like to thank Air Liquide for the project's funding. I would not have been able to complete this thesis without Dr. Dale Tree's continued guidance and advice. Lastly I would like to thank my family, friends and co-workers for all their support.

TABLE OF CONTENTS

LIST OF TABLES

LIST OF FIGURES

NOMENCLATURE

I is the intensity (W/m^2/sr/μm)

I_b is the intensity of a black body radiator (W/m^2/sr/μm)

κ is the absorption coefficient (μm^{-1})

η is the wave number (cm^{-1})

$\hat{s}$ is the path coordinate (μm)

β is the extinction coefficient $\beta = \kappa + \sigma$ (μm^{-1})

σ is the scattering coefficient (μm^{-1})

Φ is the scattering phase function

s is the path length (mm)

C_1 is a radiation constant

C_2 is a radiation constant

1 INTRODUCTION

Temperature measurements used to assess, characterize, and understand the physical processes occurring in flames are notoriously difficult to make and are of questionable accuracy. High temperatures and corrosive environments make it very difficult to acquire in situ measurements with good temporal and spatial resolution. Additionally, thermocouples are limited to temperatures below 1650°C. The most common optical method for measuring temperature is two-color pyrometry. This technique provides the solid particle temperature of either soot or burning char or some combination of the two but does not provide a gas temperature.

1.1 Objective

The objective of this work is to explore a method for measuring temperature using the infrared emission from combustion products. The focus resides in three major areas, the development of a theoretical model that provides the transfer function needed for the temperature measurement, the design and fabrication of a probe to collect the infrared emission from a flame, and experimental validation of the method comparing the optical emission measurement with a suction pyrometer temperature.

The model utilizes spectral absorption coefficients developed by (J.T. Pearson 2014) to model spectral emission as a function of gas pressure and temperature. Spectral bands are then integrated to determine the bands that can be integrated and correlated to the temperature. The probe design and fabrication consists of designing a probe that can collect emission from the

Burner Flow Reactor (BFR) at BYU. The probe will be required to collect emission in a high temperature particle laden environment and transmit the emission to a Fourier Transform InfraRed (FTIR) spectrometer for measurement. Lastly, the probe and FTIR will be used to collect emission data and using a calibration, convert voltages to intensities and produce a gas temperature which will be compared to the temperature measured by a suction pyrometer. These tests will be performed primarily in natural gas flames where soot loading is low.

1.2   Scope

As was previously discussed, the work presented in this research spans from the development of a model showing spectral emission for H_2O at different temperatures and concentrations to the collection of actual emission data from a reactor. This included: 1) The development of a method for identifying spectral bands that could be used to measure temperature and establishing a correlation between temperature and spectral emission; 2) The designing and fabrication of an optical probe; 3) The collection of data using the probe and validation using a suction pyrometer. The work used an existing reactor for the data collection portion. This work did not involve the development of the spectral absorption distribution function. It also does not include the demonstration of this technique in particle laden flames or for situations with high spatial and temporal resolution.

Future work in this area could lead to the determination of separate heat flux intensities for gaseous and particle emissions, gas species concentrations for H_2O and CO_2, and separate gas and particle temperatures. However, these outcomes are not within the scope of this project.

2 LITERATURE REVIEW

This chapter provides a literature review of current temperature measurement methods including physical probes and optical methods. While not all methods are presented, the focus is on those commonly used and those most closely related to the method being investigated. These sections provide context for the methods and results found in this research, as well as the motivation for developing a new method of temperature measurement. The most common methods employed in flames include: 1) Thermocouples; 2) Suction Pyrometers; and 3) Two-color Pyrometry. Following these methods are a variety of optical methods that employ spectral characteristics of gases to infer the temperature.

2.1 Thermocouples

Thermocouples are widely used in many different temperature measurement applications. This is due to the fact that they are inexpensive, robust and easy to implement. Thermocouples are comprised of two dissimilar conductors that contact each other at the measuring end called the bead. A temperature can be measured due to the voltage differential that is produced. One issue with directly measuring the temperature of a flame is the fact that material property limitations prevent thermocouples from measuring temperatures above 1650°C. Flame temperatures routinely exceed this limit, preventing thermocouples from taking in situ measurements. When using thermocouples in gases surrounded by cool walls, large errors due to both radiative and conductive heat loss occur (Heitor 1993). The use of fine wires removes the majority of conduction losses,

however radiative losses continue to be an issue at higher temperatures and can contribute to errors of hundreds of degrees (D. Bradley 1968). Soot particles and reactor wall temperatures higher than the gas temperature can also produce emissions which contribute significantly to radiation error when using thermocouples (F.C. Lockwood 1982). Correcting for these effects can be difficult as the uncertainties due to the convective heat transfer coefficient, the bead size, shape and emissivity as well as the temperature and emissivity of the surroundings all affect the signal (A.H.K. Sato 1975, R. Viskanta 1987). Currently no models exist that completely solve these issues, and as a result, suction pyrometers are often used for high temperature combustion environments (L.G. Blevins 1999).

2.2 Suction Pyrometers

Suction pyrometers, or aspirated thermocouples, work by extracting the combustion gases into a probe in order to pass the sample at high velocity over a shielded thermocouple. This results in a high convective heat transfer which more closely represents the actual gas temperature and avoids complications due to radiative heat losses (J.S. Newman 1979, A. Z'Graggen 2007). This method also allows for extended thermocouple life by protecting the bead from oxidizing agents or species which might react at the surface. As a result, this process is an improvement upon a bare wire thermocouple for some applications, however, a sacrifice to the spatial and temporal resolution of the measurement occurs. The level of spatial resolution as well as the accuracy of the measurement depends on the aspiration rate of the probe. At higher aspiration rates, the agreement between the thermocouple and gas temperature measurement improves, but the spatial resolution decreases significantly as the volume of the gas sampled is related to the velocity of the aspirated air. The ASTM recommended rate for the aspirated air is 5 m/s, which shows a significant improvement over an open wire thermocouple measurement, however, other sources recommend

4

rates upwards of 150 m/s in an attempt to more accurately characterize the true temperature (L.G. Blevins 1999). Smaller burners are not able to support such high aspiration rates due to the volume flow rate required. Even with high aspiration rates, time response can be an issue as the probe can take up to 3 minutes to reach equilibrium temperature and then 1 minute for every change in 100°C (S.C. Kim 2008). In solid fuel flames, molten ash particles can produce rapid deposition, which can become a problem as the sampling probe can become clogged and will not allow for the desired flow velocity (L.G. Blevins 1999).

2.3   Two-color Pyrometry

Two-color pyrometry is an optical method that compares two colors of the visible broadband spectrum in order to determine a temperature. Initially this method was applied along a single line of sight using band pass filters and detectors. More recently, the method has been demonstrated and used with a color digital camera where each pixel in the camera acts as a detector. An RGB camera records intensity values for the red, blue and green light collected for each pixel. Each pixel is evaluated and analyzed in order to determine a respective temperature and an emissivity. This method has been known to work well in applications with broadband emission and is widely used. The main drawback of this method is the fact that it works only when solid particles such as soot, coal or ash are present. It also provides only a line-of-sight result that is weighted toward the higher temperatures along the line. Gray or spectrally dependent radiative emission models are necessary to process results (T. Draper 2012). While this method can be applied successfully to objects that fit the gray body assumption, coal flames have been found to be more complex and the models used to determine temperature show significant temperature differences when compared to each other (T. Draper 2012).

2.4   Coherent Anti Stokes Raman Spectroscopy (CARS)

A method known as Coherent anti-Stokes Raman Spectroscopy (CARS) has been investigated as a possible method for determining temperature and concentrations in combustion environments. CARS combines three coherent beams (a probe beam, pump beam, and stokes beam) to produce a coherent excited beam. Because this excited beam is coherent and at a specific wavelength, the signal can be isolated using optical filters. This relatively large signal strength has the potential to be larger than background or particle radiation. The measurement volume being made of intersecting laser beams provides good spatial as well as excellent temporal resolution (R.L. Farrow 1982). The primary disadvantages to this method include the need for laser sources that have excellent intensity stabilization, optical alignment, and a fairly complicated and expensive experimental setup and significant post processing of the data (R.L. Farrow 1982). CARS has only been demonstrated in coal flames assisted by natural gas which reduces particle loading and interference. It has not been demonstrated in unassisted coal flames, and is difficult to implement in industrial settings.

2.5   Infrared Spectral Analysis

While there are many other techniques employed to measure temperature, this section focuses on those most similar to the new method being investigated, or methods which employ spectral band emission from gases.

The initial concept of measuring temperature from gas rotational spectra was introduced in 1977 by Griffith and Anderson (R.J. Anderson 1977). Two methods were used to measure the temperature of CO between the ranges of 300-425 K with an FTIR. The first method used peak values of measured CO spectra and compared them against stored spectrum of an empty test cell, the second used line width calculations. These methods resulted in excellent error levels at room

temperature with steadily increasing error as the temperature increased to 425 K (R.J. Anderson 1977). The first method of least-squares regression fit for peak values of absorbance lines was demonstrated on pure CO_2 by infrared absorption spectroscopy just over a decade later using an electrically heated gas cell at temperatures ranging from 363-463 K (L.A. Gross 1988). At the same time, work was being done that reported the use of CO_2 emission measurements to infer gas temperature on a coal flame using emission transmission spectroscopy (P.R. Solomon 1988). This work used the peak emission from the 4.3 μm (2325 cm^{-1}) band of CO_2, and fit a Planck, black body, intensity function to the measured spectra to infer temperature. The approach requires the concentration of CO_2 to be high enough that the absorption coefficient is unity for a significant fraction of the band. This also prevents the data from being used to determine CO_2 concentration.

High-resolution transmission data of CO_2 using a heated gas cell have been measured, however thus far the data has been used to compare against and validate line by line high temperature CO_2 absorption models, not for the measurement of temperature and not for combustion products (Evseev 2012).

Recently, Modest et al. developed a method which utilizes a radiation model and FTIR measurement to infer temperature (T. Ren 2013). In this method, the model and measurement spectrum are compared by adjusting CO_2 concentration and temperature in the model until they fit the measured spectrum. The model predicts the transmissivity of CO_2 as would be measured by an FTIR as a function of pressure, temperature, concentration and path length. The temperature and concentration are then varied in the model until the predicted spectra best fits the measured spectra. The resolution used is 4 cm^{-1} for CO_2 in N_2.

An experiment using a shock tube system was used to diagnose the possibilities of using H_2O bands to determine temperature and concentration in scramjet engine flows (T.E. Parker

1996). Known mixtures of H_2O, N_2, O_2, and Ar were shock heated to temperatures ranging from 1400 K to 3000 K and measured data were compared to known band models. The temperature was determined by fitting modeled spectra to the measured data and using the temperature which provided the best fit. While this demonstrated the use of the spectra to obtain temperature, the concentration of gases needs to be known in order to use the method.

Clausen (1996) performed optical temperature measurements using CO_2 as the subject gas with a water cooled probe, optical fiber, and FTIR. Measurements of emission were taken near the 2350 cm^{-1} band, and as with work done by Solomon et al. (P.R. Solomon 1988), the peaks of the CO_2 band emissions were fit with a Planck curve to infer temperature. The experiment mapped the cross section of a 1.3 MW reactor and data were validated using a suction pyrometer, good agreement was observed between the suction pyrometer and the optical measurement (Clausen 1996).

More recently, an optical probe measuring a lignite coal flame in a 77 kW_{th} reactor was used to measure particle radiation using a least squares regression fit of a Planck curve on the broadband sections of the measured spectra. Gas temperature was not calculated from CO_2 or H_2O emission bands. The experiment showed that within the coal flame region, particle radiation was the dominant radiation source due to high particle densities (D. Backstrom 2014).

2.6   Current Approach

The method proposed in this work differs significantly from all other methods previously discussed in that this technique will ratio the measured integrated spectral signal over bands of 100-150 cm^{-1} between 5185 and 5800 cm^{-1} and then utilize the ratio of those integrated bands to infer the temperature. The relationship between the ratio of band emissions and temperature is determined through the modeled integrated emission. Previous methods used direct line

8

comparison of collected spectra or Planck curve line fitting with a unity assumption. These methods require data acquisition at high resolution and the uncertainty is dependent on the absolute value of the calibration. Any deposition on the probe or misalignment of optical components that alter the signal produce a shift in the inferred temperature. In other methods, it is assumed that CO_2 emissivity is unity, limiting the method to instances where higher concentrations of CO_2 are present. The use of an FTIR is necessary for these methods, limiting commercial application. By utilizing the integrated ratios, the need for spectral resolution and precise measurement of the spectrum with the FTIR is reduced. The ratio method also reduces the need for absolute calibration of the detectors and optical system and enables the technique to be used in future work with optical filters and detectors, without the need for an FTIR. Using filters and detectors would increase the temporal resolution of the method dramatically and allow for response times of less than a second without the need for post processing to determine the temperature. This flexibility is a major improvement and allows for the method to be commercially viable in future iterations.

3   BACKGROUND

This chapter provides the background information needed to understand and evaluate the integral band method for temperature measurement. The chapter begins by reviewing the radiative transfer equation and the assumptions applicable for this application that enable a solution relating the measured intensity to the temperature and concentration of H_2O. A discussion is then provided describing how a model was used to determine the relationship between the ratio of integrated band intensities and the temperature.

3.1   Radiative Transfer Equation - Theory

Radiative emission from participating media can be characterized by the radiative transfer equation shown in Equation (3.1).

$$\frac{dI_n}{ds} = \kappa_n I_{b,n} - \beta_n I_n + \frac{\sigma_{s,n}}{4\pi} \int_{4\pi} I_n(\hat{s}_i)\Phi_n(\hat{s}_i, \hat{s})d\Omega \tag{3.1}$$

Assuming scattering to be negligible the equation simplifies to:

$$\frac{dI_n}{ds} = \kappa_n I_{b,n} - \kappa_n I_n \tag{3.2}$$

Negligible scattering is an excellent assumption for gases and is normally acceptable for soot particles because their size is so small that the concentration must be unusually large for scattering. This assumption is also typically good for most combustion flows because the concentration of the larger particles is relatively low compared to the fine particles for which scattering is negligible. In this work, particles were not present except for a few exploratory cases.

10

A further assumption of a uniform temperature and a uniform absorption coefficient along the path, s, produces the solution shown in Equation 3.3.

$$I_n(s) = I_{b,n}(1 - exp(-\kappa_n s)) \tag{3.3}$$

Where:

$$I_{b,\eta} = \frac{C_1}{\pi * \eta^5 * \left(\exp\left(\frac{C_2}{\eta T}\right) - 1\right)} \tag{3.4}$$

$$\kappa_n = C_{abs}\frac{P_i N_A}{RT} \tag{3.5}$$

and C_{abs}, P_i, R, N_A and T are the absorption cross section, partial pressure, Avogadro's number, the ideal gas constant and absolute temperature respectively.

By definition, a flame is a region of high temperature and concentration gradients and therefore the uniform temperature assumption is only valid in post flame regions. The assumption is also more likely to be valid in post flame regions where the path length is short. The measurements obtained in this work will be done in post flame regions of uniform temperature and concentration over a long path length (750 mm). Future work will look at reducing the path length and quantify errors associated with non-uniform temperature and species distributions.

The absorption cross sections required to produce an intensity from a known concentration and temperature were obtained from the work of Pearson (2013) who used the Voigt profile and the spectroscopic data from the HITEMP 2010 database (L.S. Rothman. I.E.G 2010). The cross sections were tabulated according to pressure and concentration at intervals of 0.005 cm^{-1}.

Figure 3.1 shows the spectral intensity for CO_2 (10%) and H_2O (10%) at an optical path length of 0.5m at 1200 K using the spectral absorption cross sections developed by Pearson (2013). These concentrations and temperatures are values similar to those expected in the products of coal

and natural gas flames and therefore provide some indication of the spectral regions where IR emissions will be highest for these gases.
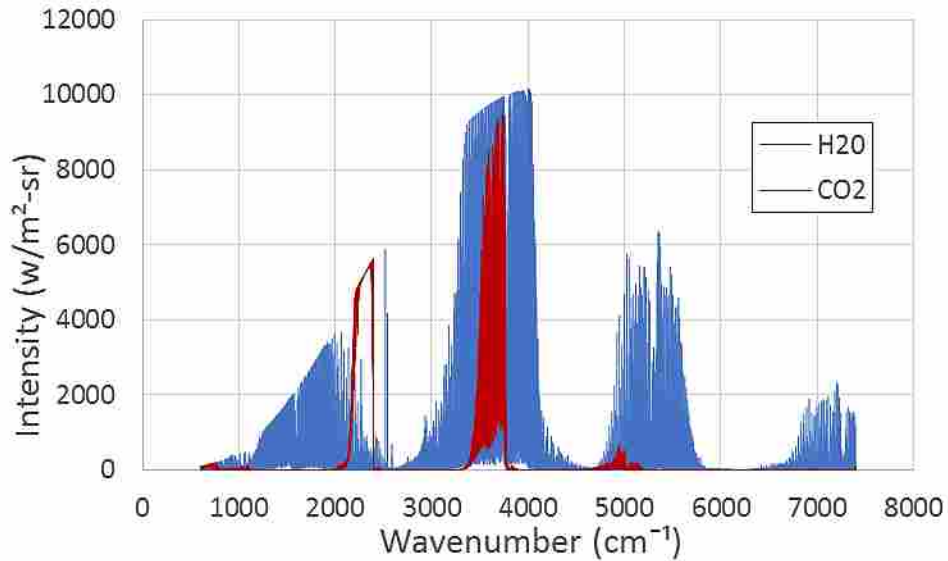
Figure 3.1 – CO₂ and H₂O emission intensity between 600-7400 cm⁻¹ at a temperature of 1200 K, optical path length of 0.5m, pressure of 1 atm, and a concentration of 10%

Inspection of these gaseous emissions allows for a better understanding of the temperature measurement methods discussed previously. For CO_2 in the $2100 – 2400$ cm⁻¹ region and for H_2O between 1100 and 2000 and between 3500 and 4200 cm⁻¹, many of the emission peaks are saturated and the bands take on the shape of the Planck distribution. As discussed earlier, existing techniques by Clausen et al. (Clausen 1996) and Solomon et al. (P.R. Solomon 1988) fit these regions with the Planck equation (Equation (3.4)) to obtain a gas temperature. This can work well when the combined concentration and path length are large but cannot be utilized over smaller path lengths and lower concentrations.

Ren et al. (T. Ren 2013) changed temperature and concentration in their model of the gas transmission in an attempt to match the measured transmission spectra in the FTIR. This technique is challenging because the FTIR truncates and shifts the individual spectral line peaks as a result

of the Fourier Transform process used to measure the data. This requires Ren et al. (T. Ren 2013) to also transform the modeled spectrum in order to match the measured result.

The method proposed in this work develops a relationship between the ratio of two integrated spectral bands and the temperature. Both processes, integration and the use of a measured ratio rather than an absolute value, result in a reduction of possible error associated with the use of emission measurements for temperature. Utilizing an integrated spectral band also enables the emission data to eventually be collected with a single detector and band pass filter rather than requiring detailed spectral data. The approach used here is to determine and test appropriate bands with the FTIR and then utilize band pass filters and detectors in future work.

3.2   Spectral Band Selection

The spectral bands were selected by a study of the modeled spectrum and by testing numerous integrated ratios and their relation to temperature. Saturated bands were not necessary with the ratio method used in this work.

The FTIR has a preferred range of 600-7400 cm⁻¹ when using an MCT detector coupled with a KBr beam-splitter. This enables collection over the entire spectrum shown in Figure 3.1. The collection of IR emission from hot H_2O and CO_2 requires that there is no absorption of colder H_2O and CO_2 between the gas and the detector. This is most easily accomplished by the use of optical fibers. While expensive optical fibers can be found which transmit in the longer IR wavelengths, inexpensive optical fibers are available with a transmissivity above 90% within 4545 to 25000 cm⁻¹. Focusing on the region between 4545 and 7400 cm⁻¹, in Figure 3.1, it can be seen that H_2O will produce a stronger signal than CO_2. Furthermore, CO_2 will produce a significant fraction of the emission in the range from 4545 to 5185 cm⁻¹ that would interfere or add to the H_2O signal. It was therefore decided to focus on the H_2O emission between 5185 and 5800 cm⁻¹ which is shown

13

as an isolated region in Figure 3.2. The desired spectral region will vary based on the optimal optical transmissivity of the equipment used.
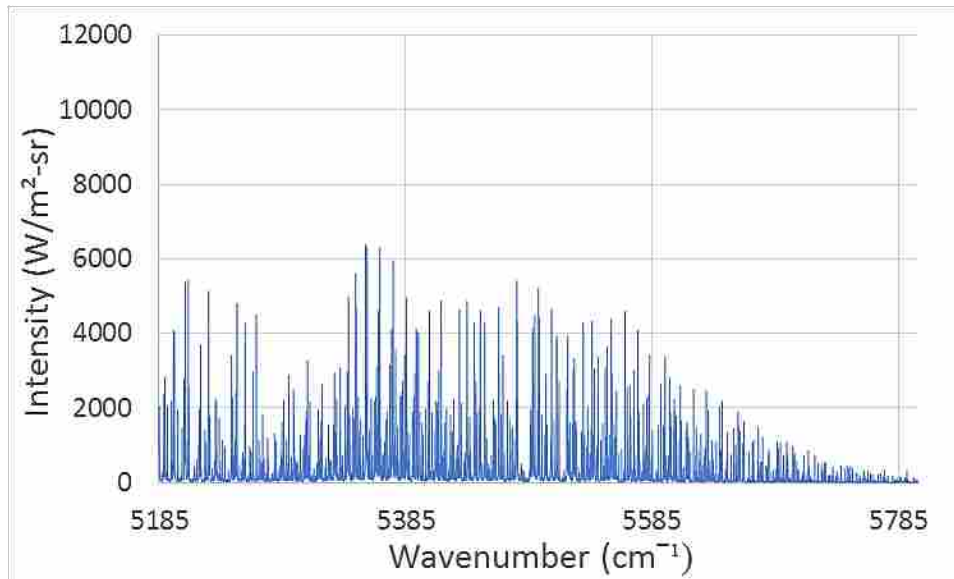
Figure 3.2 – H₂O emission intensity between 5185-5800 cm⁻¹ at a temperature of 1200 K, optical path length of 0.5m, pressure of 1 atm, and a concentration of 10%

Once the spectral region was selected, bands, or subsections were chosen somewhat arbitrarily, in order to create subsections of equal size. It was desired to select a large enough band that a line would not dominate the signal and to avoid phase shift influence, but small enough that several bands could be considered. Figure 3.3 shows five different bands selected which are identified by letters A through E. The numerical values for each band are given in Table 3.1.
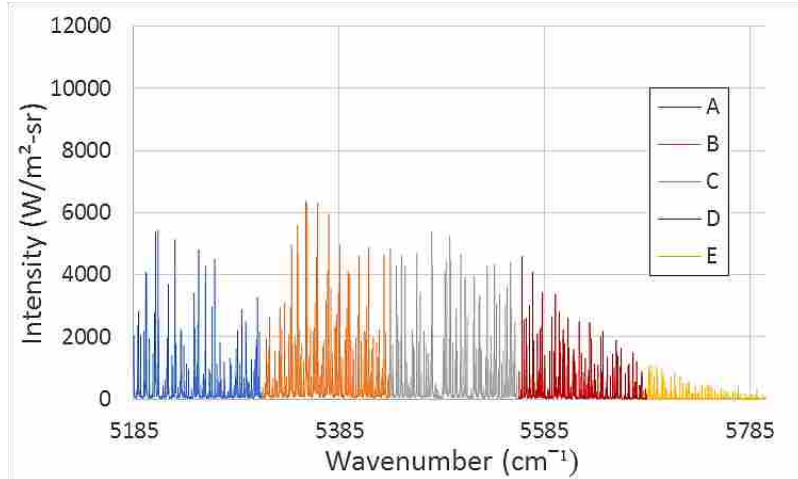
Figure 3.3 – H₂O emission intensity between 5185-5800 cm⁻¹ at a temperature of 1200 K, optical path length of 0.5m, pressure of 1 atm, and a concentration of 10%, split into subsections A-E by color

Table 3.1 – Subsections and their wavenumber bands

Section	Range (cm⁻¹)
A	5185-5310
B	5310-5435
C	5435-5560
D	5560-5685
E	5685-5800

Once the bands were chosen, the sections were integrated numerically using Newton's method as shown in Equation (3.6):

$$I_{band} = \int I_v dv = \sum_{v_1}^{v_2} I_{v_i} \, \Delta v_i \qquad (3.6)$$

Which reduces to Newton's method:

$$I_{band} = \sum_{v1}^{v2} I_v \, \Delta v_i \qquad (3.7)$$

The integral values for each band were then compared using ratios in order to determine if there was a correlation between temperature and resultant intensity:

$$R_{a/b} = \frac{I_{band,a}}{I_{band,b}} \qquad (3.8)$$

15

Results for three pairs of integral bands as a function of temperature are shown in Figure 3.4. With five bands, ten possible correlations can be made. All possible correlations for the chosen bands have been tested, however, this work focuses on E/A, E/B and E/C due to several factors. As can be seen in Figure 3.4, these ratio pairs produce monotonic functions where a single temperature is associated with a specific ratio of integrated band emissions. In addition to this, the slope is favorable with the ratio changing a significant and easily measurable amount over the temperatures of interest. Some of the other ratio pairs produced exponentially changing ratios which were with a small slope at low temperature rapidly transitioning to a steep slope. Temperature ratios using region D looked favorable and were initially utilized but for unknown reasons the integrated value of "D" relative to the other integral regions seemed to be larger than predicted. For a given set of data, all three correlations should be in agreement. Any deviation between the correlations indicates a form of bias error.
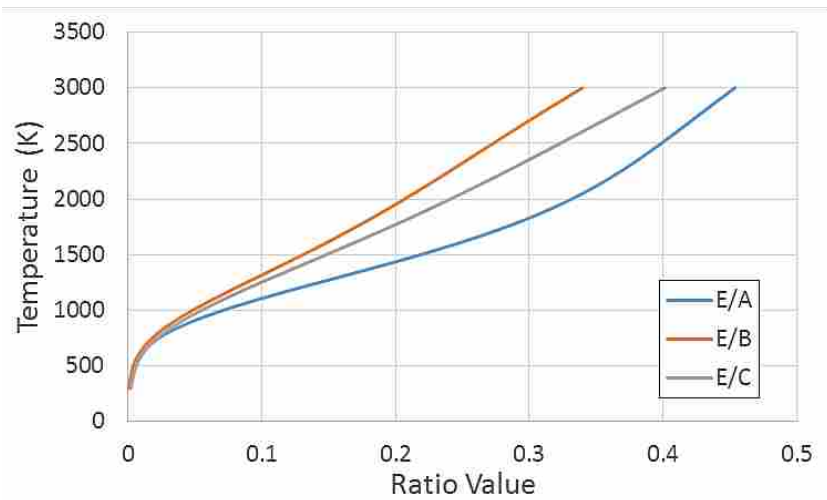
Figure 3.4 – Correlation lines for the ratios E/A, E/B, and E/C between 300 – 3000 K

The integrated band values were tested at multiple concentrations of H_2O in order to determine the sensitivity of the correlations with respect to changing concentration. Figure 3.5

demonstrates an increase in intensity with concentration over band A. This increase of magnitude with concentration can be seen with band A-E, and is effectively removed once Equation (3.8) is applied as can be seen in Figure 3.6 for the integrated band ratio of E/B. These data are representative of all integrated bands as well as each ratio combination used in this work.
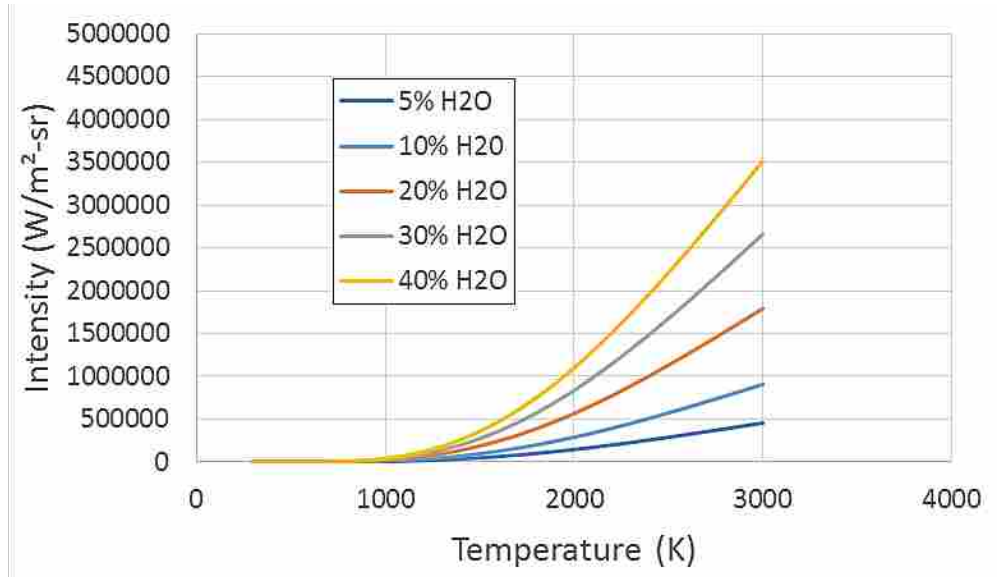
Figure 3.5 – Intensity values for integrated band A for increasing concentrations of H₂O
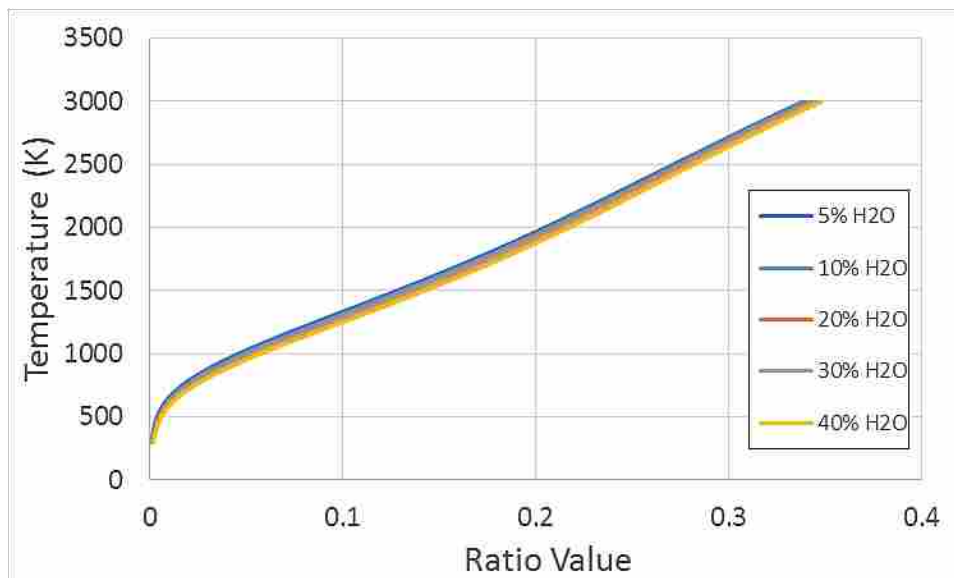
Figure 3.6 – Integrated band ratio E/B values for increasing concentrations of H₂O

4   EXPERIMENTAL SETUP

This chapter will describe the experimental apparatus and operating conditions used to calibrate the optical pyrometer and to collect the demonstration data.

4.1   Probe Design and Calibration

Absorption of water vapor emission by cold water vapor between the measurement volume and the detector (self-absorption) will interfere with the measurement. As a result, a probe including an optical path free of interference was needed. This was accomplished by creating a probe that could be inserted into a water cooled jacket adjacent to the measurement volume with the intent to focus incident intensity into an optical fiber. The fiber acted as a conduit to deliver the intensity to an FTIR spectrometer which was purged with nitrogen. The probe was able to view the horizontal distance 0.75 m across the reactor. Future testing will involve a cold target and shorter path lengths but in these tests the probe was positioned where the temperature profile was expected to be relatively constant across the diameter of the reactor. The probe tip design shown in Figure 4.1 includes the housing, a focusing lens, and the optical fiber. The probe was purged with argon to avoid absorption by cold gases within the probe. The lens and fiber holders were fabricated out of stainless steel. A plano-convex lens made of calcium fluoride, with a focal length of 25 mm, and a diameter of 12.7 mm is located within the probe. Calcium fluoride was selected as the lens material because of high transmittance in the IR region as seen in Figure 4.2.
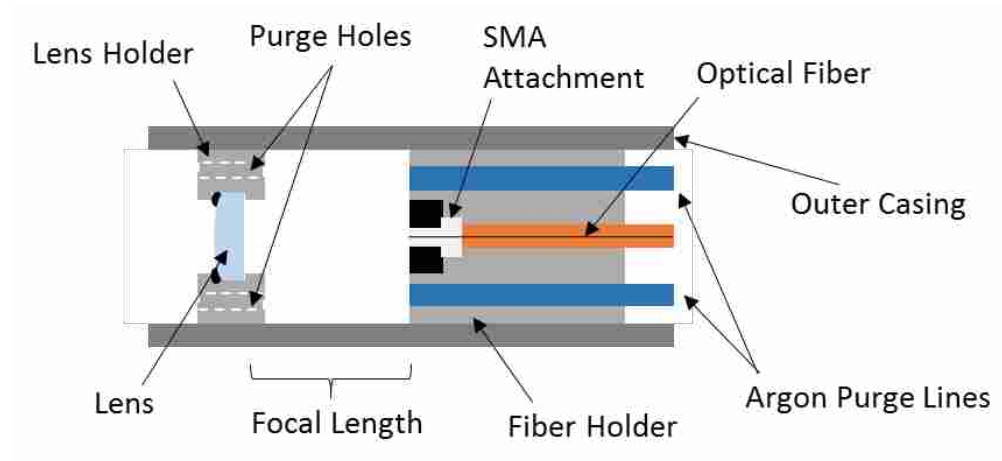
Figure 4.1 – Diagram of optical probe comprised of outer casing, lens holder, lens, fiber holder, fiber, and argon purge lines
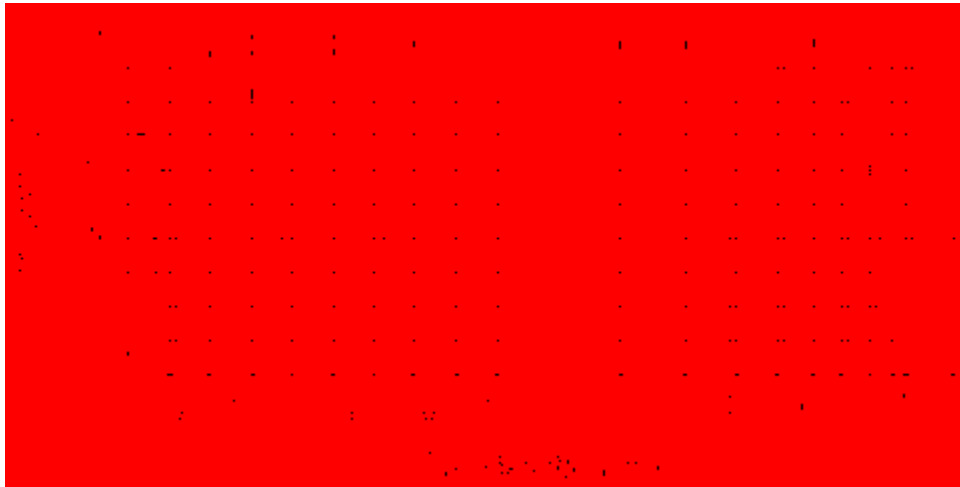
Figure 4.2 – Transmittance of calcium fluoride between 0-10 µm

The optical fiber is pure silica, Ø400 µm, 0.39 NA, SMA-SMA Fiber Patch Cable, 2 meters in length purchased from Thorlabs (item no. M28L02). The design of the probe allows any SMA-905 fiber coupling to be easily attached or detached in case there is a need to change the type of fiber or replace the existing fiber due to damage. In addition, the distance between the lens and the fiber can be adjusted with set screws which allows for different focal lengths in case the lens is changed or replaced. In order to assure that the fiber was positioned at the focal length of the lens,

measurements were calculated and the fiber was shown to produce a peak signal with the FTIR when placed in front of a Black Body Emitter. With the fiber placed at the focal length of the lens, the collection of the emission of the gas will be a column perpendicular to the lens. In order to reduce particle build up and to assure a lack of self-absorption within the water cooled jacket, a low flow Argon purge was used to inhibit flow into the probe. The light collected was then delivered to the FTIR as shown in Figure 4.3.
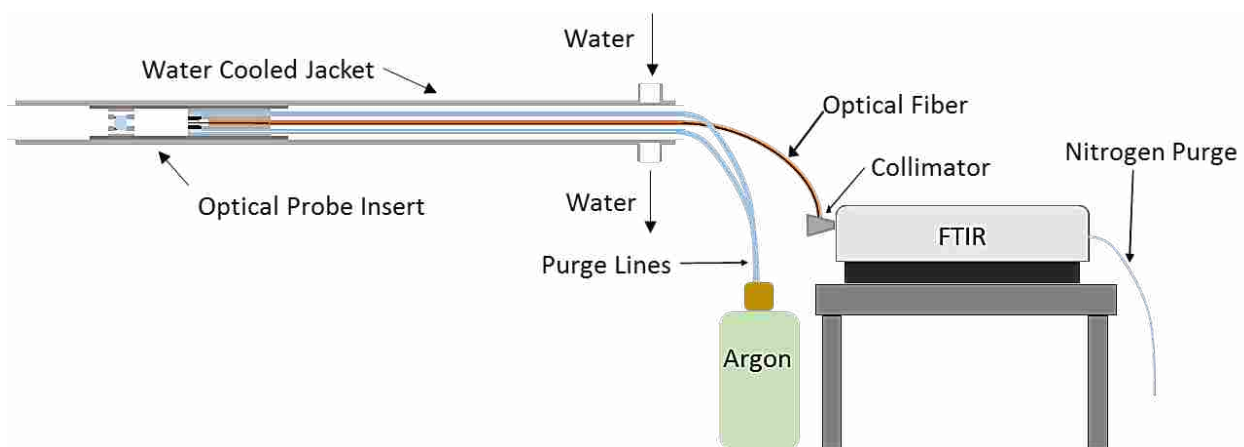
Figure 4.3 – Optical Pyrometer and FTIR interface

The SMA fiber attachment that is not connected to the probe will be connected to a collimator just outside the FTIR that has an SMA fiber attachment. The collimator will transmit a collimated beam of light to the interferometer within the FTIR. The FTIR then performs a Fourier transform on the light source, converting it into a voltage signal as a function of wavenumber. In order to minimize self-absorption effects, a nitrogen purge was used within the FTIR.

Before data collection could begin, the probe signal needed to be calibrated with a Black Body Emitter (BB). The probe was recessed 20.3 cm from the end of the water cooled jacket, which was placed in front of the BB cavity at a known temperature to produce a measured signal that was compared to a calculated Planck curve. An Argon purge was used in the probe, and a

Nitrogen purge was used in the FTIR during calibration in order to minimize self-absorption. The object of the calibration process was to account for the transmittance loss of the system (including lens, fiber, and air absorption) and the sensitivity of the FTIR detector as a function of wavenumber in order to accurately determine intensity. The results of the calibration are given in the results section.

4.2   Conditions of Data Collection

Once calibration was complete, testing was performed on the BFR with a methane flame. The BFR is a 150 kW$_{th}$ down-fired, refractory lined, water cooled, cylindrical furnace. Figure 4.4 shows a partial schematic diagram of the combustion facility as well as the experimental setup used to collect data.
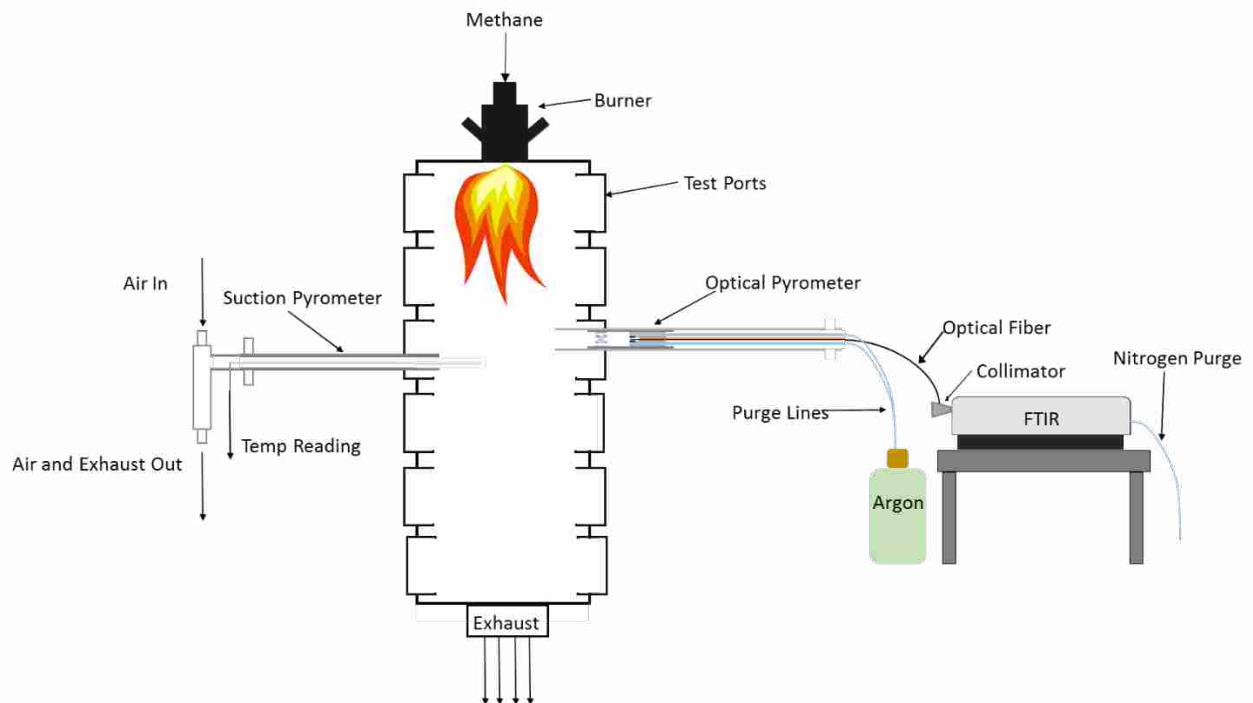
Figure 4.4 – Experimental setup featuring the BFR, Optical Pyrometer, Suction Pyrometer and the FTIR

Validation of the data was achieved by using a suction pyrometer with a type K thermocouple in conjunction with the optical probe. It should be noted that the suction pyrometer was used on the same side of the reactor in the same location as the optical pyrometer, but the two measurements were not taken at the same time. Each measurement was taken beginning at start-up when the natural gas flame was first lit and the walls were initially at ambient temperature. The fuel and air flow rates were constant for each test and it was assumed that the reactor heated at the same rate each time. Figure 4.4 depicts the probe and suction pyrometer on the opposite sides to enable labeling. In order to have a sufficient rate of convection to avoid radiation loss, the ASTM standard for suction pyrometer flow rates is 5 m/s, but studies have shown that radiative losses are lower as the flow rate increases (L.G. Blevins 1999). For this reason the suction pyrometer was operated at a flow rate of 40 m/s, the maximum flow rate possible by the eductor and air pressure available. The suction pyrometer was inserted into the lower half of the third port, approximately 105 cm from the burner exit, and data were collected at 10 cm intervals starting at the edge of the interior wall in order to assess the validity of the uniform temperate assumption. As was previously addressed, suction pyrometers attempt to reduce radiation error, which cause a gas temperature to be artificially low (in the direction of the wall temperature) and the spatial resolution of the measurements is quite poor due to the large flow rates. Due to the fact that the flow rate of the suction pyrometer is limited by existing equipment design, the measured temperature is expected to be slightly less than the actual temperature of the combustion gases, but the amount is difficult to determine. The suction pyrometer along with a calculated adiabatic flame temperature based on the operating condition were used as reference points to determine the reasonability of the optically determined temperature.

The three operating conditions listed in Table 4.1 were selected in order to provide a simple way to change temperature without changing probe position. The fuel used was natural gas which was modeled as methane for the calculation of adiabatic flame temperature. The three operating conditions were tested in two ways by both the suction pyrometer and the optical pyrometer. The first test was a time progression documenting the reactor warming up from the time of ignition to approximately 240 minutes. The second test was performed once the reactor reached steady state. Due to the fact that the testing of the two pyrometers was executed in the same location, they were performed sequentially over two days for each condition. Multiple tests were performed at steady state for each condition in order to determine the variability of the methods.

The air entering the reactor was preheated to an average temperature of 500°F (approx. 533 K) using an electric heater and was used as the reactant temperature in calculating the adiabatic flame temperature. The temperature of the gases in the reactor should be well below the adiabatic flame temperature due to large heat losses in the reactor, however, the adiabatic flame temperature provides a limit for the temperature difference that is produced by the change in equivalence ratio and some indication of how large that temperature difference might be.

Table 4.1 – Test conditions using the BFR

Condition	Methane (SCFH)	Air (kg/hr.)	Equivalence (ϕ)	Adiabatic Flame Temp (K)
1	300	200	0.600	1664
2	350	200	0.715	1862
3	400	200	0.820	2024

The optical probe was inserted into the water cooled jacket and tests were performed with the probe recessed 20.3 cm from the end of the jacket. Argon was used to purge the 20.3 cm of the recessed portion of the water cooled jacket with a flow rate such that a positive pressure was created and self-absorbance was minimized. The assembly was inserted into the BFR in the lower

half of the third window from the top, on the south side of the reactor (approximately 105 cm from the burner exit). This location was chosen due to the fact that the visible flame did not reach the line of sight of the probe at the majority of the conditions, thereby making soot free measurements possible. However, at 400 SCFH methane, the sooting flame was observed to occasionally appear in the measurement volume.

The assembly was inserted into the BFR such that the optical path length of the signal was the entire width of the reactor (0.75 m). Data were collected with a nitrogen purged FTIR using an external collimator, a KBr beam-splitter, and the MCT detector. The maximum FTIR resolution setting (0.125) was used which corresponds to data spacing of 0.06 cm^{-1} for the aforementioned range of 5185 to 5800 cm^{-1}. This resolution was chosen in order to more closely approximate the resolution seen in the model correlations.

Once the data were collected, Equations (3.7), (3.8) and (5.3) were used in conjunction with background radiation removal (discussed in the following section) in order to determine a resultant temperature. The results of the calibration process, the BFR experiments, and an uncertainty analysis will be discussed in the following section.

5   RESULTS AND DISCUSSION

Results include calibration, development of a transfer function, and example temperature measurements in the BFR. A comparison of optical and suction pyrometer temperatures, the need to remove background radiation, and the uncertainty of the proposed method will all be discussed.

5.1   Calibration

During calibration, the collection probe and optical fiber were placed in front of a black body cavity close enough that the collection angle of the probe only includes the black body surface of the cavity. The measured voltage (M_η) at a given wavelength is given by Equation (5.1), where: ε_b, is the emissivity of the cavity (assumed to be 1.0), $I_{b,\eta}$ is the Planck black body intensity at the known temperature of the radiating cavity, A_l is the area of the collection lens, S_η is a constant representing the sensitivity of the FTIR in converting incident intensity to output voltage, and τ_η is the spectral transmittance of the optical fiber. The lens area, spectral sensitivity and fiber transmittance were combined into a single constant, C_η, to be found by the calibration.

$$M_\eta = \varepsilon_b I_{b,\eta} A_l S_\eta \tau_\eta = \varepsilon_b I_{b,\eta} C_\eta \tag{5.1}$$

Figure 5.1 shows the measured FTIR signal from black body emission at 1100ºC and a Planck blackbody intensity equation plotted as a function of wavenumber for the same temperature. The shape of the measured signal differs from the Planck curve because of the spectral dependence of the detector response and the spectral dependence of the transmittance of the receiving optics and optical fiber. Also despite purging the FTIR and the optical probe, a small

layer of cold air was present between the collection optics and the black body. This air contained H_2O and CO_2 vapor which can be seen as spectral absorption bands between 3700 – 4000 cm^{-1} and 5100 – 5600 cm^{-1}. This self-absorbance is not present in experiments because the probe is inserted in a water cooled jacket into the hot combustion products and the cooled volume within the probe is purged with argon.
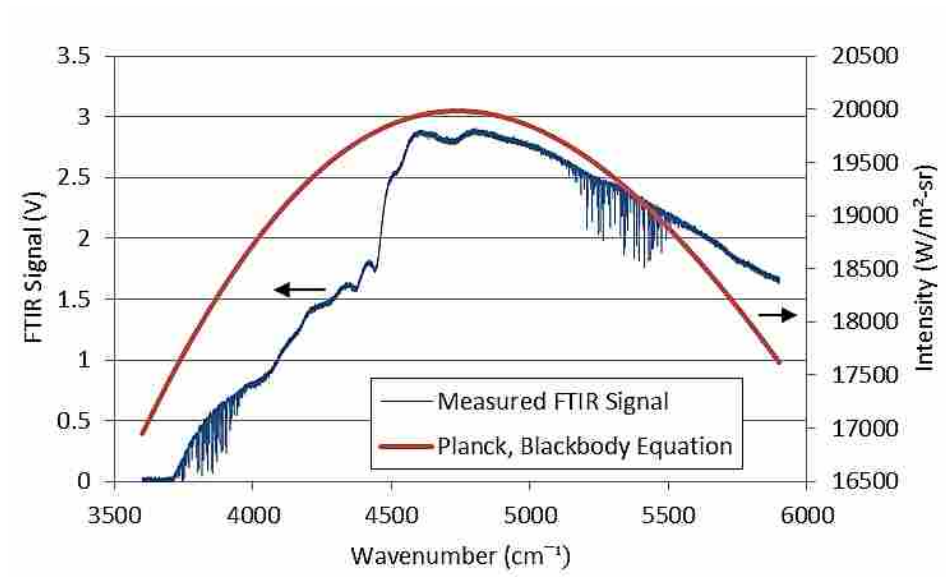
Figure 5.1 – Measured FTIR signal at a BB temperature of 1100°C (approx. 1373 K) from 3600-5900 cm^{-1} with the calculated Planck curve at the same temperature

In order to calculate a transfer function relating FTIR signal output to intensity, the spectral region between 5018-5900 cm^{-1} was used as shown in Figure 5.2. This region is larger than the region where measurements were collected in order to facilitate curve fitting the data in regions where self-absorption was not present. The influence of the H_2O absorption was removed by fitting the measured signal data with a smooth function as shown in Figure 5.3.
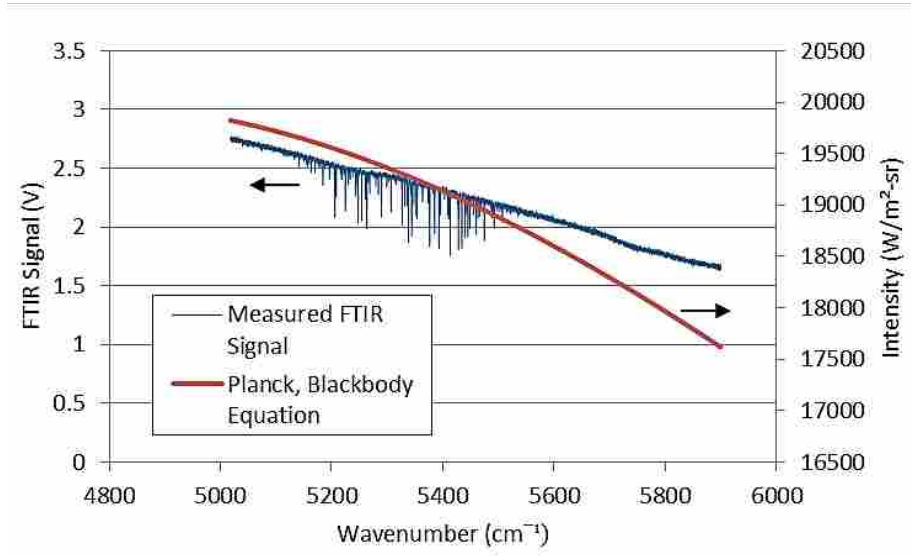
Figure 5.2 – A comparison of the FTIR signal versus the calculated Planck equation
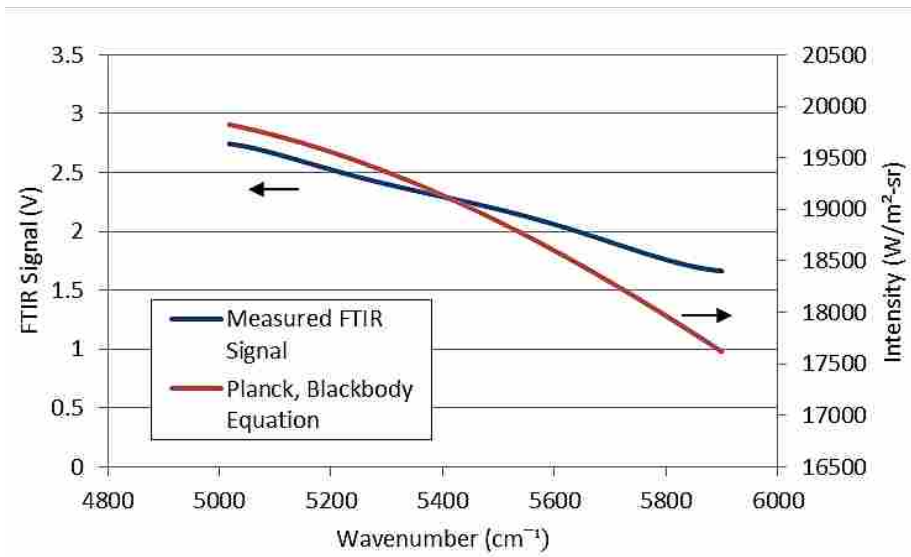
Figure 5.3 – A comparison of a smooth FTIR signal versus the calculated Planck equation

The spectral ratio of measured data to blackbody intensity was then used to define the spectral transfer function, C_v, as shown using the following equation:

$$C_v = \frac{M_v}{I_{b,\eta}} \frac{Volts}{W/m^2/sr} \tag{5.2}$$

The measured C_v for three blackbody temperatures are shown in Figure 5.4. The figure shows that the FTIR detector is not linear with incident intensity but the shape of the spectral

27

response is similar. The C_v used in this work is unique to the experimental setup used in this work and takes into account the unique optical setup combined with the FTIR used to collect data. Because the transfer function is dependent on the temperature or intensity of the emission and that temperature is unknown, the selection of the transfer function becomes an iterative process. A guessed temperature is used to provide the initial transfer function and the resulting temperature is used to determine the new transfer function. Fortunately, given the fact that the temperature is dependent on the ratio of intensities and not the absolute temperature, there is little error involved in guessing a temperature for the transfer function, on the order of 1% for an initial guess without iterations. The iteration process converges rapidly and allows an absolute intensity to be determined.

The algorithm for determining temperature from a measured FTIR voltage is completed as follows:

- A guessed temperature is used along with calibration constant C_v for that temperature to provide the spectral intensity as shown in Equation (5.3).

- The spectral intensity is then integrated numerically over the spectral bands A thru E as shown in Figure 3.3 according to Equation (5.3).

- Ratios of integrated band intensities are then calculated for various combinations of bands as shown in Equation (3.8).

- The temperature for a given band ratio is then calculated according the theoretical correlations shown in Figure 3.4

- The temperature obtained is compared to the guessed temperature. If they are not within a tolerance limit, the process is repeated starting with the new temperature.

The equations used for the iteration process are shown below:

$$I_v = \frac{M_v}{C_v} \tag{5.3}$$

$$I_{band} = \int I_v dv = dv * \sum_{v1}^{v2} I_v \tag{3.8}$$

$$R_{a/b} = \frac{I_{band,a}}{I_{band,b}} \tag{3.9}$$
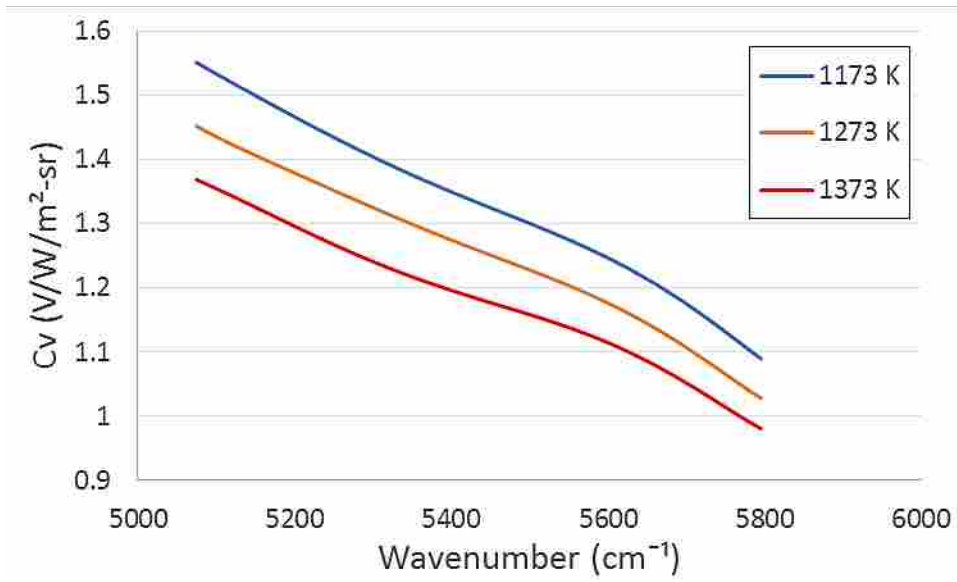
Figure 5.4 – C_v values at various calibration temperatures

5.2 Data Collection

Once the calibration process was completed, data were taken with the suction pyrometer using the method previously outlined at steady state. Results obtained with the suction pyrometer as a function of radial position for the three operating conditions are shown in Figure 5.5. The temperature across the majority of the reactor is uniform but the temperature is lower near the walls. Note the temperature increased as the amount of natural gas was increased and the overall fuel air mixture becomes closer to stoichiometric. Temperature differences in the adiabatic flame temperature between Conditions 1 and 2 is on the order of 200 K and about 160 K between Condition 2 and 3, however the change in suction pyrometer temperature is lower, on the order of

29

60 K, with slightly larger difference between Conditions 1 and 2 than seen between Conditions 2 and 3. This smaller difference between suction pyrometer data compared to the adiabatic flame temperature data is consistent with the fact that a large amount of heat is lost to the reactor walls and the temperatures are all well below the adiabatic flame temperature. Data taken with the optical pyrometer were taken at a position 10 cm from the wall edge to avoid absorption in the low temperature region and allow emission to be collected from a constant temperature region.
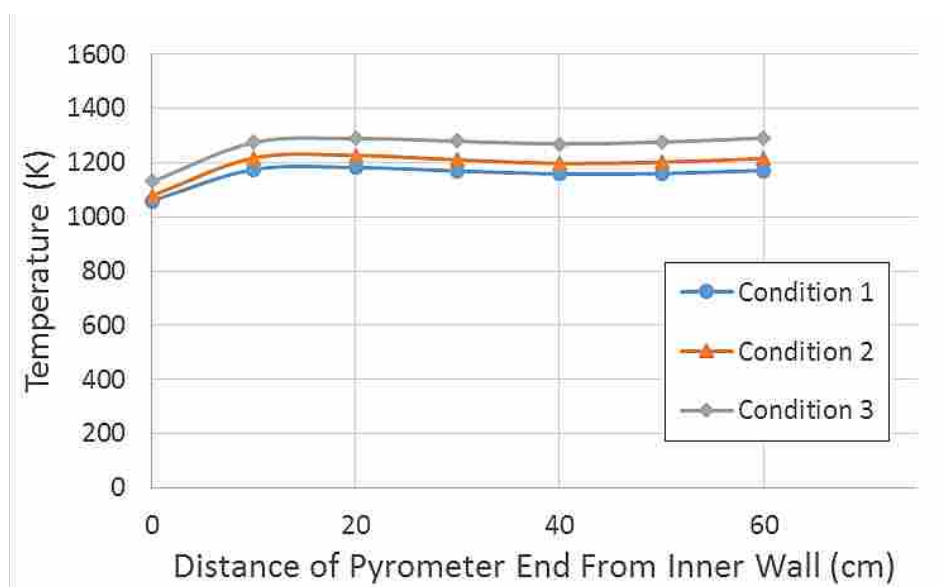
Figure 5.5 – Temperatures measured with the suction pyrometer

The following figures show raw spectral data from the FTIR in the region 3600 - 5800 cm^{-1} for the three operating conditions. Spectral emission lines from H_2O are apparent. As a general rule, as the temperature of the gas increased from Condition 1 to Condition 3, the magnitude of the intensity also increased (note the scales on each graph are different). This is an indication that the emission is increasing with increasing temperature. The relative size of the noise also decreases with increasing temperature as would be expected.

The spectral region between 4200-4800 cm^{-1} and above 5700 cm^{-1} do not show absorption from H_2O but instead indicate the level of broad band emission from background walls or soot particles. At low temperature, these emissions are relatively low but as the temperature increased, as was the case for Condition 3, the background emission became more apparent (above zero). Because this background solid surface emission is additive to the gas emission of interest, it must be removed from the data. This can be done by eliminating the hot background during data collection or by subtracting the broadband emission from the signal during data processing.
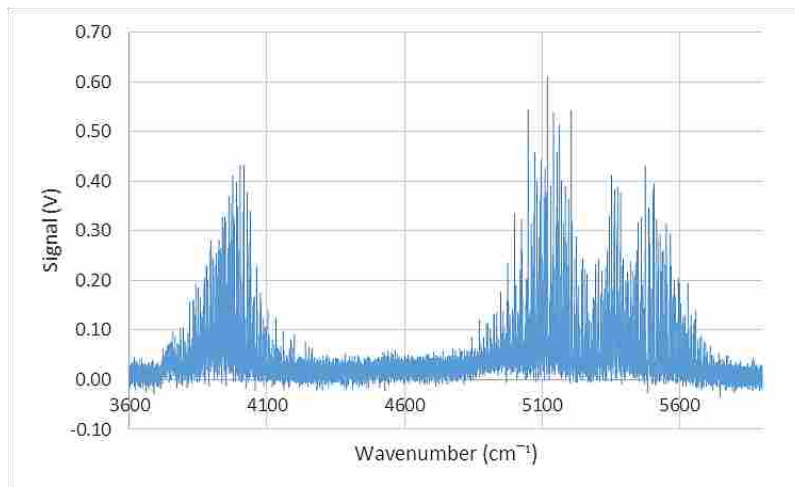
Figure 5.6– FTIR measured signal for Condition 1
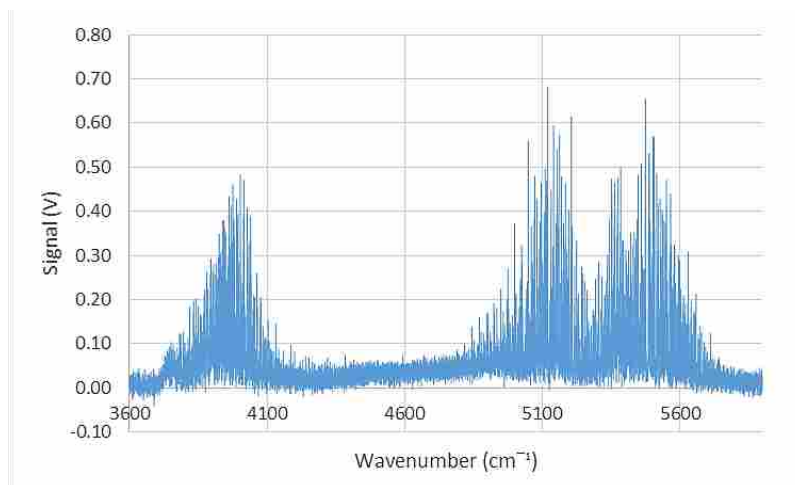
Figure 5.7 – FTIR measured signal for Condition 2
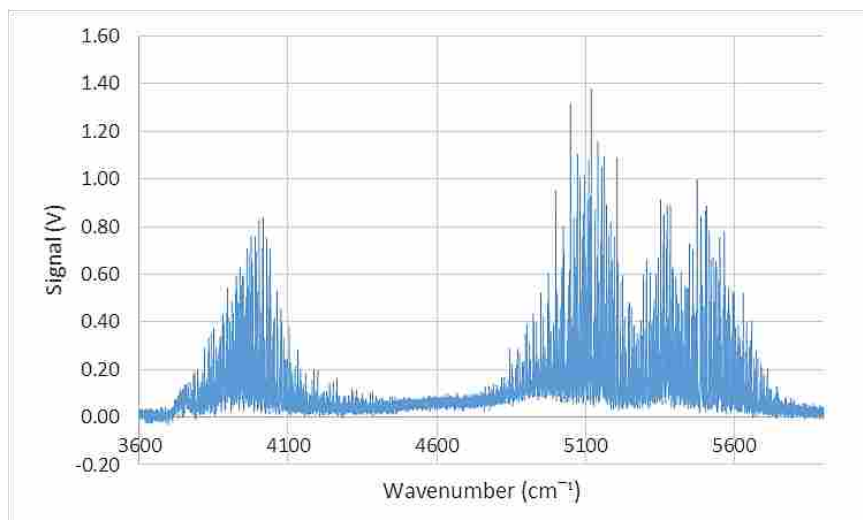
Figure 5.8 – FTIR measured signal for Condition 3

5.3   Discussion

The magnitude of the measured signal increases as temperature and H_2O concentration increases. The ratios of integrated bands remove concentration effects as discussed earlier, and the resulting change in integrated band ratio values can be fully attributed to a change in temperature.

The raw data show evidence of broadband emission coming from sources other than the desired emission from H_2O. The amount of broadband emission was observed to depend primarily in the length of time the reactor had been running suggesting it could be attributed to emission from walls which are slow to heat. These emissions were also observed to increase dramatically when the flame was observed to move into the path of the measurement. Data without broadband emissions should be centered at zero magnitude in regions where H_2O and CO_2 do not emit.

In order to remove this background signal, a method was developed to remove the broadband radiation based on the assumption that it had a Planck intensity with an emissivity value independent of wavenumber, i.e. a gray body emission. Possible explanations for the source of this interference that fit with a gray body assumption include radiation from the opposite wall as well as soot radiation from the flame itself.

32

The method used to remove this background emission involved selecting an appropriate temperature for the Planck curve which fit through the two sections (bands) of the data were chosen that exhibited zero emission from H_2O or CO_2 to be used to fit the background emission with a Planck curve as shown in Figure 5.9. Two parameters, the temperature and emissivity of the Planck equation were varied to produce the minimum least squares difference between the equation and the data. The green line represents the best fit Planck equation through the data in red. The Planck spectral intensity was then subtracted from the data at all wavelengths to produce the broadband corrected results shown in Figure 5.10. After the subtraction was performed, the red spectral regions are seen to be centered on a null magnitude instead of the initial offset value (approx. 800 w/m²-sr). The offset values seen in the data varies from case to case. Once the data has been corrected and the broadband radiation removed, the intensity data can be integrated to determine the resultant gas temperature.
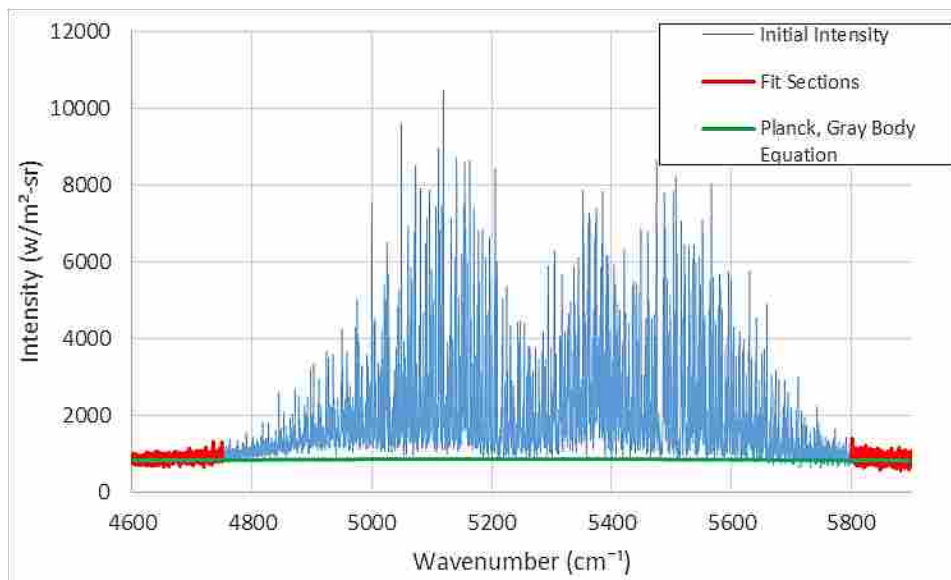
Figure 5.9 – Intensity data showing two gray body fit sections (red) with the proposed gray body Planck line for correction (green)
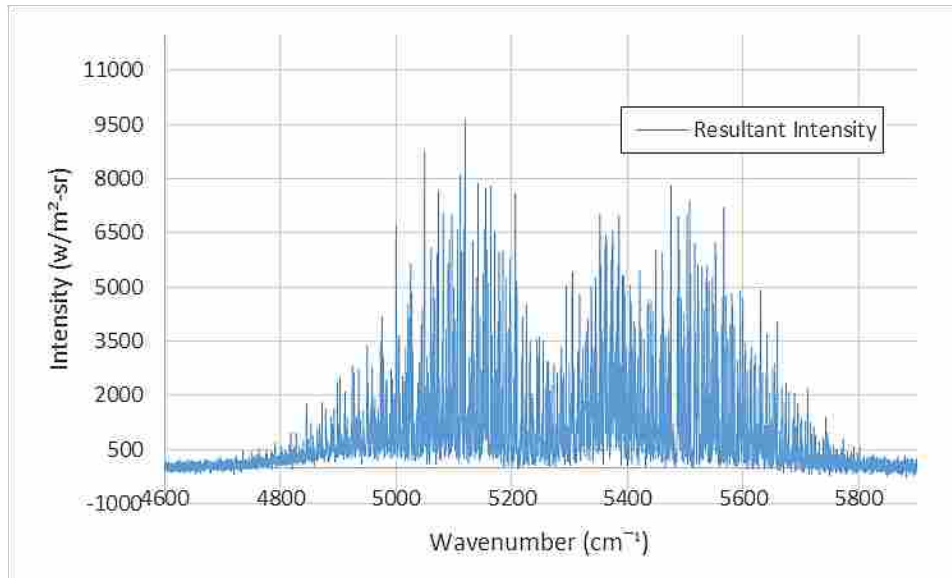
Figure 5.10 – Corrected intensity data

The influence of broadband emission removal can be seen by comparing temperature results with and without removal. Figure 5.11 shows measured optical temperature, calculated for each of three different integral ratios, E/A. E/B, and E/C as a function of time for Condition 1 without broadband removal. Also shown in the figure is the wall temperature of the reactor section where gaseous emissions were collected (Wall Temp 3). The optical temperatures increase steadily with time until they exceed the calculated adiabatic flame temperature for this condition (1664 K). It can be seen that the optical data follow the same trend as the increasing wall temperature suggesting that the wall emissions are influencing the gas measurement. It is also important to note that one of the three integrated band ratios (E/A) produced a temperature significantly lower than the other three indicating the integrated emissions are not solely from H_2O.

34
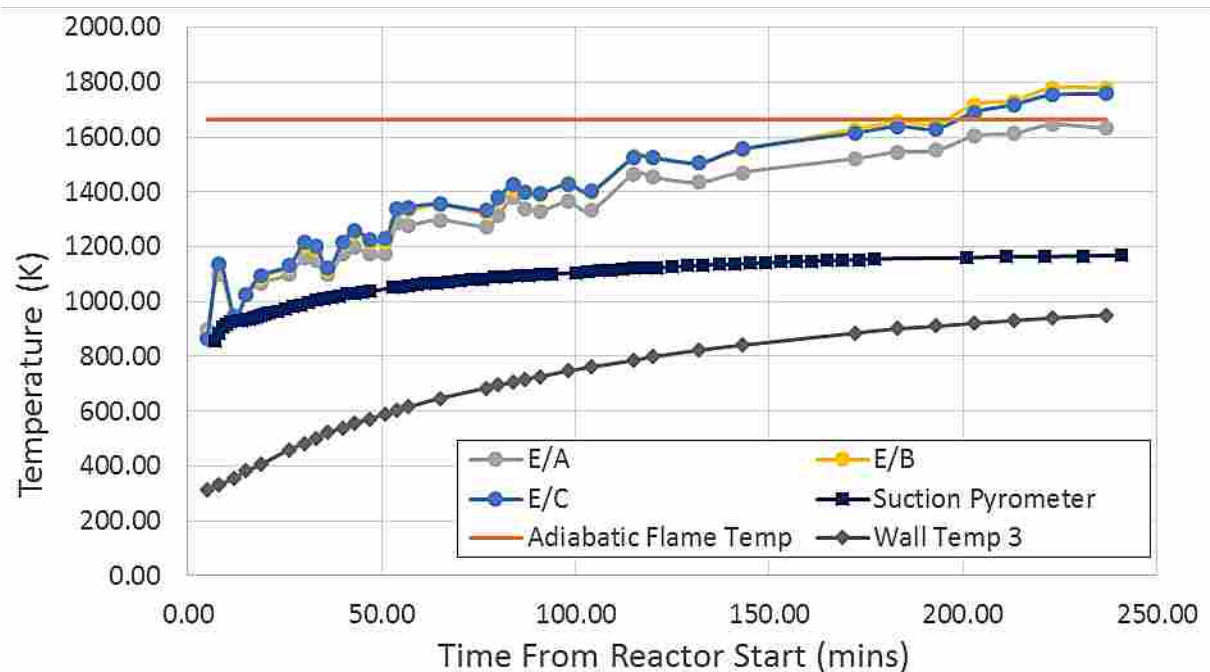
Figure 5.11 – Resultant temperatures for Condition 1 during a startup time progression for the three integrated ratio pairs without background correction compared to the suction pyrometer, adiabatic and wall temperature, time (x-axis) is from the initial ignition of the reactor

Figure 5.12 shows the same time progression for Condition 1 but with the broadband emission removed. Note that the temperatures determined for each of the three spectral pairs are now in good agreement, and they also follow the trend of the suction pyrometer rather than that of the wall temperature. The measured gas temperatures are well below the adiabatic flame temperatures as would be expected in a water-cooled reactor with relatively high surface area to volume ratio. The change in optically measured temperature with the removal technique is seen to be more significant at higher wall temperatures. The fluctuation in temperature at the beginning of startup is likely due to poor signal to noise ratio at lower gas temperatures for this condition. Tables for all time resolved data can be seen in the Appendix.
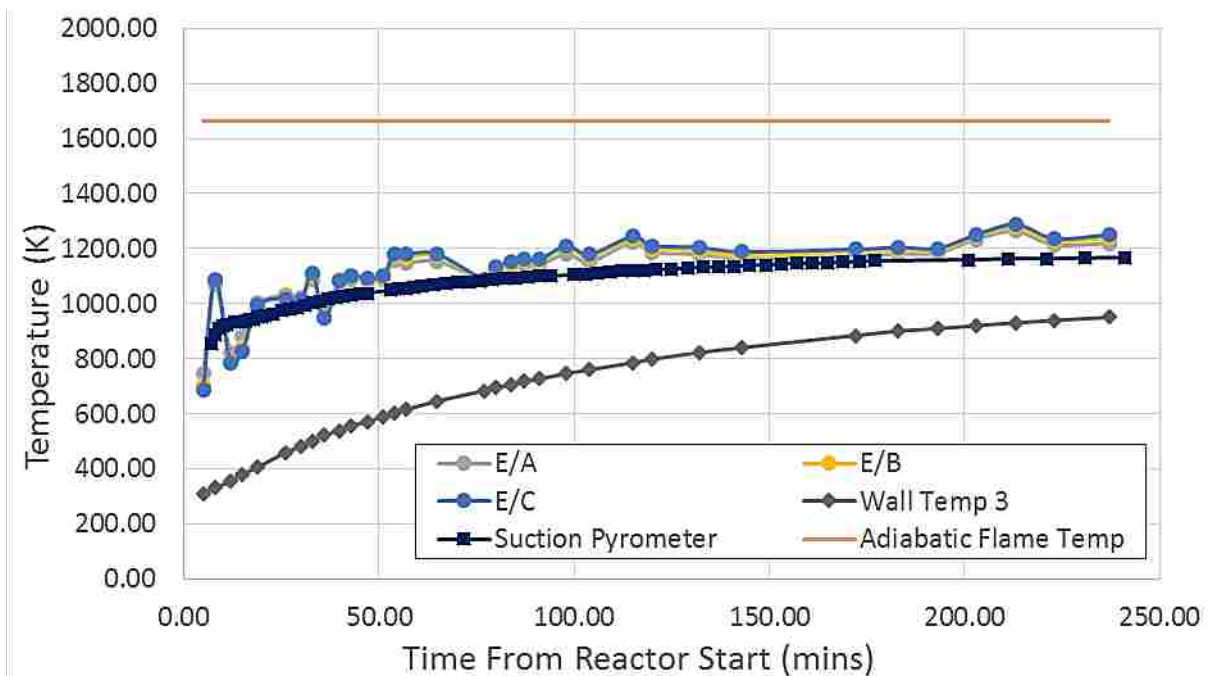
Figure 5.12 – Resultant temperatures for Condition 1 during a startup time progression for the three integrated ratio pairs with background correction compared to the suction pyrometer, adiabatic and wall temperature, time (x-axis) is from the initial ignition of the reactor

The following figures show the same experiments performed at the remaining two conditions. Similar trends before and after background removal can be seen. Note that at higher temperatures, fluctuations in optically measured data are reduced due to the improved noise to signal ratio. The absence of data for Condition 2 between 200 and 250 minutes is due to a temporary failure of the FTIR during that time period. It is apparent that the background radiation present during this experiment had a significant effect on integrated ratios of intensity. As a result, all of the temperature calculations for these conditions require background removal and will be reported with the correction.
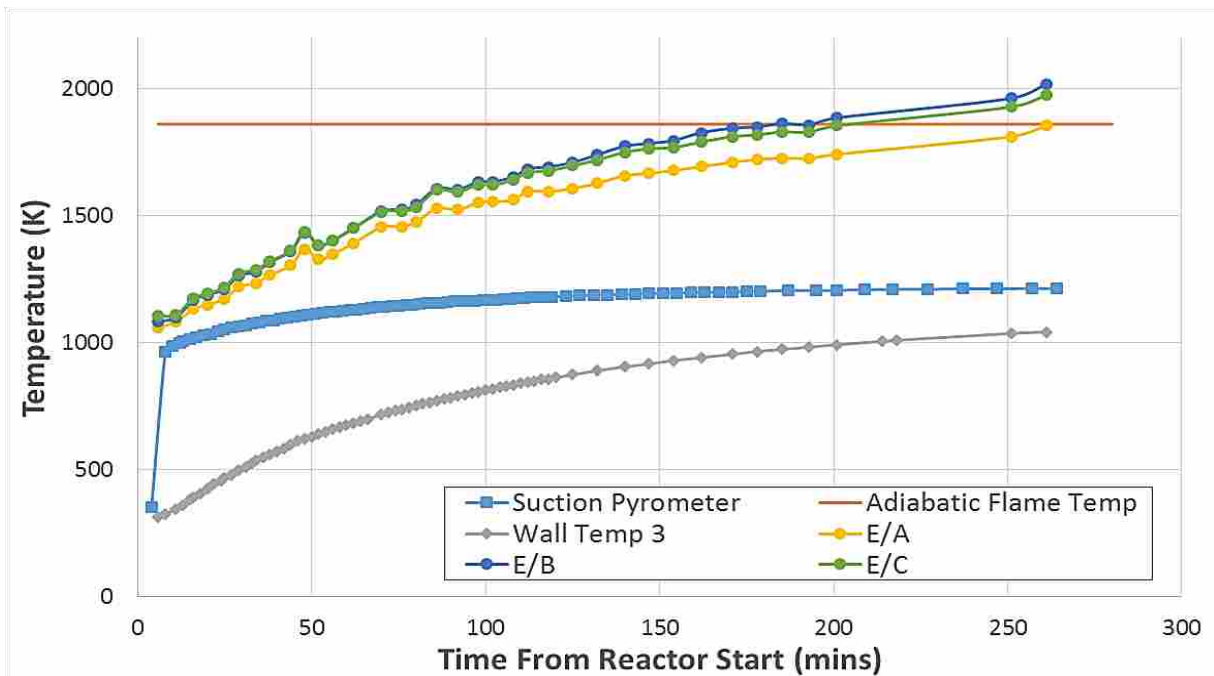
Figure 5.13 – Resultant temperatures for Condition 2 during a startup time progression for the three integrated ratio pairs without background correction compared to the suction pyrometer, adiabatic and wall temperature, time (x-axis) is from the initial ignition of the reactor
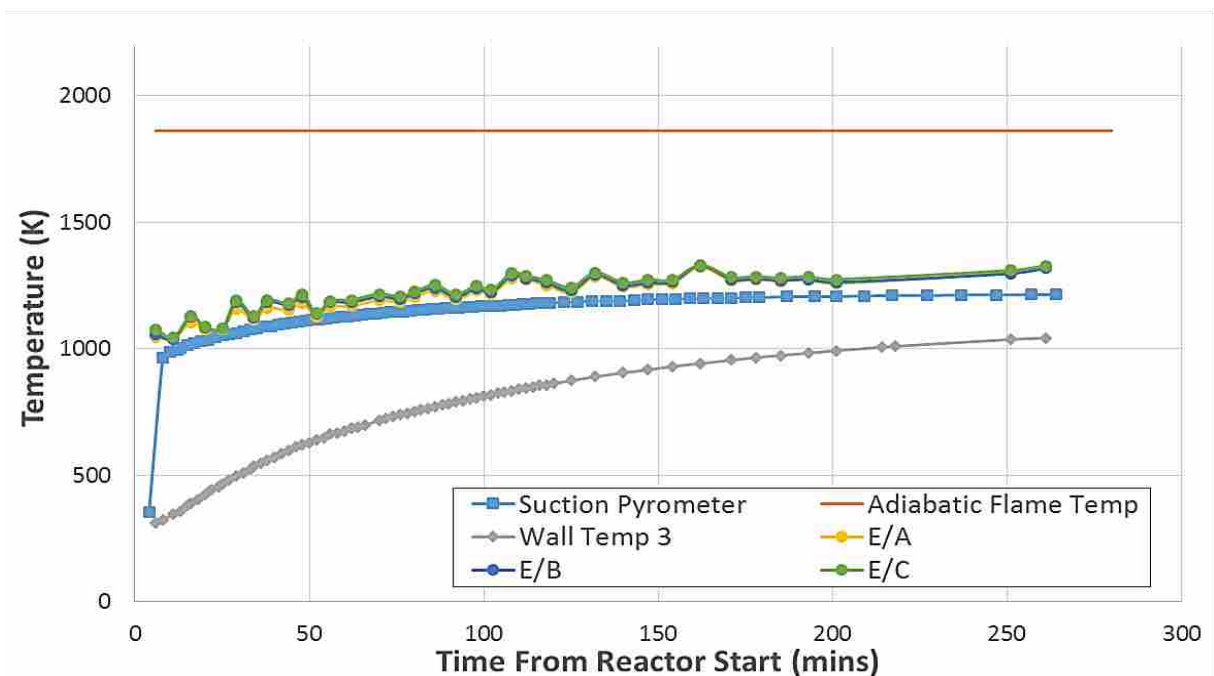
Figure 5.14 – Resultant temperatures for Condition 2 during a startup time progression for the three integrated ratio pairs with background correction compared to the suction pyrometer, adiabatic and wall temperature, time (x-axis) is from the initial ignition of the reactor

37
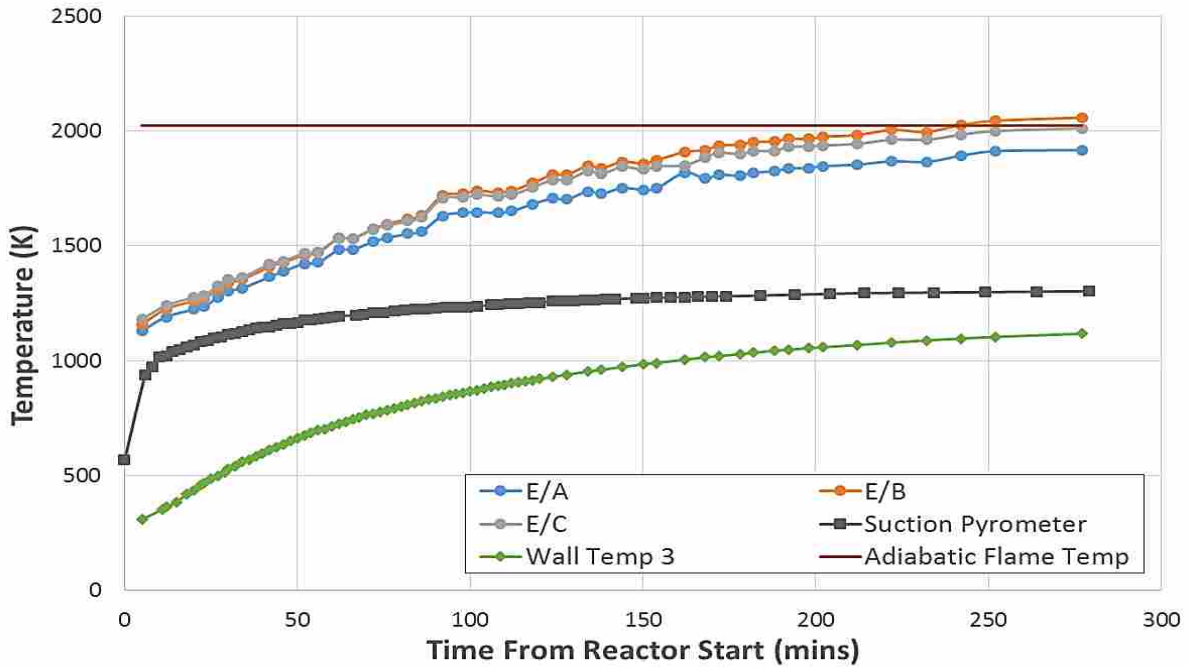
Figure 5.15 – Resultant temperatures for Condition 3 during a startup time progression for the three integrated ratio pairs without background correction compared to the suction pyrometer, adiabatic and wall temperature, time (x-axis) is from the initial ignition of the reactor
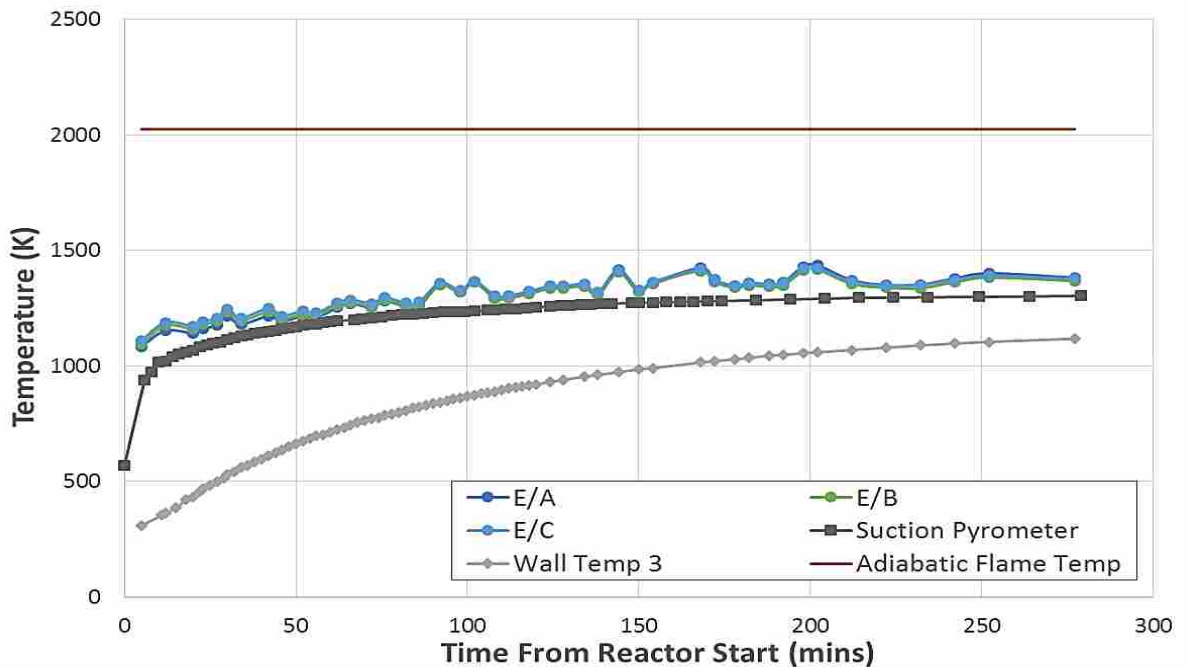
Figure 5.16 – Resultant temperatures for Condition 3 during a startup time progression for the three integrated ratio pairs with background correction compared to the suction pyrometer, adiabatic and wall temperature, time (x-axis) is from the initial ignition of the reactor

38

For the broadband removal process, a Planck curve is generated based off of a best fit with temperature and emissivity as dependent variables. Table 5.1 contains the average temperature determined for the Planck curve fit for each condition at steady state. Wall temperatures measured by a thermocouple embedded in the refractory below the slag layer is also listed. Because broadband radiation increased slowly over time and correlates with the increase in wall temperature, it make sense that the broadband radiation is coming mostly from the walls and the Planck temperature should be related but at higher equivalence ratios, the flame became elongated and soot radiation from the flame increased. This increased the probability that some of the broadband radiation could be coming from the soot or from a reflection of soot radiation off of the walls and into the probe line of sight. Given this possibility, the Planck curve fit temperatures seem very reasonable and could be useful in determining total radiation measurements.

Table 5.1 – Steady state values of the broadband removal temperature for all three conditions compared to the wall temperature

Condition	Equivalence Ratio	Broadband Temp (K)	Wall Temp (K)	Difference (%)
1	0.600	897	909	1.3%
2	0.715	964	974	1.0%
3	0.820	984	1095	10.2%

Table 5.2 contains a comparison of the optically measured and suction pyrometer temperature data at steady state for the three conditions. The relative percent difference between the optical measurement and the suction pyrometer is also listed. Excellent agreement is observed. In all cases the optical data are slightly higher than the suction pyrometer data as might be expected. The differences range from 3.2% to 3.6%.

Table 5.2 – Steady state values of the three integrated ratio pairs for all three conditions compared to suction pyrometer temperatures with background correction

Condition	Equivalence Ratio	Optical Temp (K)	Suction Pyrometer Temp (K)	Difference (%)
1	0.600	1200	1161	3.2%
2	0.715	1274	1228	3.6%
3	0.820	1337	1292	3.4%
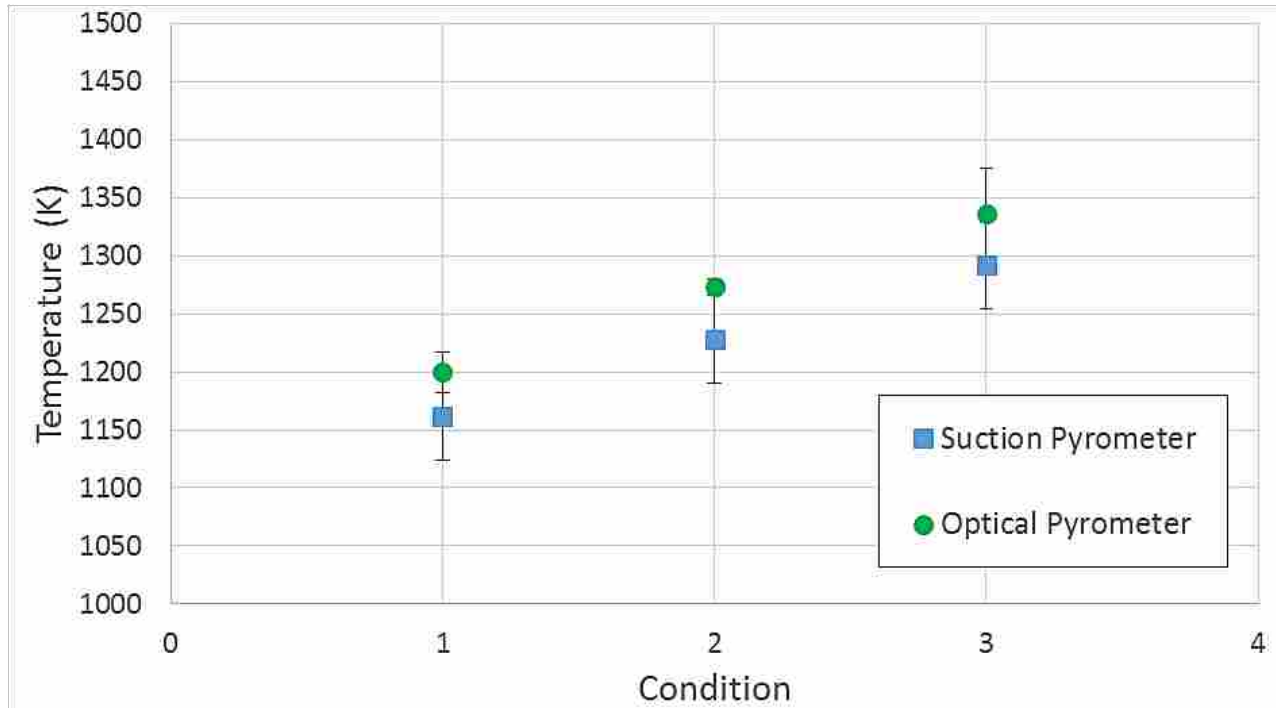
Figure 5.17 – Steady state data of the three integrated ratio pairs for all three conditions compared to suction pyrometer temperatures with background correction

Figure 5.17 shows the average of eight data points for each condition taken at steady state and compared to suction pyrometer temperatures taken at identical conditions. The error bars represent the magnitude of one standard deviation.

Although the error bars for the two methods overlap indicating no significant difference in the two measurements within their range of uncertainty, the optical measurements were consistently 3% higher than the suction pyrometer. As discussed in the literature review, suction pyrometers are expected to be lower than the actual gas temperature when wall temperatures are lower than gas temperatures because of radiation losses. In this case the velocity of gases passing

over the shielded thermocouple were on the order of 50 m/s which is well above the ASTM suggested velocity and therefore the suction pyrometer temperatures are expected to be reasonably accurate. Given this understanding of thermocouple temperature errors, it is possible that the optical temperature is more accurate than the suction pyrometer.

5.3.1 Uncertainty

Uncertainty in measurements consists of two components, bias error and random error. The bias error is related to the calibration accuracy and the amount of offset produced by interfering factors. For example, the broadband emission biased the emission from the H_2O and caused considerable error before it was removed. Another potential source of bias error exists in the calibration process and subsequent changes to the optical system. For example, if the lens were to become dirty and transmit light differently during the measurement than during calibration. Another source of bias error is the unknown concentration of the H_2O. While taking the ratio of integrated intensities cancels most of the error associated with this issue, large uncertainties in H_2O such as 40% H_2O vs 5% H_2O lead to uncertainties in the temperature of 0.25%. The best measure of bias error that could be produced was to compare the optical result to the best known temperature of the gas which was obtained with the suction pyrometer. This uncertainty is on the order of $\pm$ 3% based on differences between the two measurements. Another method of looking at bias error is to consider the differences between the temperature calculated by two different band ratios, such as E and A vs. E and B. Theoretically these bands should produce identical temperatures and the extent to which they are different is an indication of bias errors in the calibration and measurement or in the theoretical development. In the case of the data obtained here, this uncertainty was on the order of 1-2% which is smaller than the uncertainty obtained by comparing the optical and suction pyrometer techniques.

The second type or error is due to random uncertainties produced by the noise or variations in the measurement. This can be evaluated by the assessing the repeatability of the measurement. Assuming the temperature to be changing in a smooth continuous fashion, the time progression data are a good indication of the random uncertainty. When temperatures are low, the variation in temperature from one time to the next is considerably larger than later time periods when the temperature is higher and the signal to noise ratio of the FTIR improves. Thus the random uncertainty is a function of the temperature being measured. At high temperatures (1200 K), this uncertainty is on the order of 1-2% as shown in Table 5.2 but the uncertainty becomes larger, $\pm 8\%$ at lower temperatures (850 K).

In order to approximate a total uncertainty, the root mean square of bias and random uncertainties was calculated as shown in Table 5.3. The result is a total uncertainty of approximately 4% for high temperatures (above 1200 K) and approximately 9% for low temperatures on the order of 850 K. At temperatures above 1000 K, the uncertainty of this technique is a good as that of any other known temperature measurement technique.

Table 5.3 Calculation of the total uncertainty at two temperatures

Source of Uncertainty	Error at 850 K	Error at 1200 K
Calibration and Modeling	3%	3%
Integrated Spectral Emission (Spectral Model)	2%	2%
Random Signal to Noise	8%	2%
Total Error (RMS)	8.8%	4.1%

6 SUMMARY AND CONCLUSIONS

A method for measuring temperature using the integrated intensity of H_2O emission bands has been developed and demonstrated on a 150 kW_{th} natural gas flame using a fiber optic based probe and FTIR. The development and demonstration produced the following results:

- A spectral model of H_2O emission was developed from the spectral absorption coefficients produced by Pearson (2013). The model produced the emission along a line of sight of uniform temperature and H_2O concentration.

- The model was used to investigate numerous spectral bands until several pairs were found which produce a monotonic relationship between the ratio of integrated band intensity and temperature.

- The ratio of spectral band intensities was found to be relatively insensitive to H_2O concentration with differences on the order of 0.25% for a concentration range of 5 to 40 %.

- A collection probe was designed, fabricated and tested for the collection of gaseous emission along a line of sight using a lens and optical fiber within a water cooled jacket.

- A method was developed to provide a calibration transfer function relating FTIR output to radiative emission input. The transfer function was found to be dependent on the incident intensity and therefore iteration is required to determine the proper transfer function for a given temperature.

- The optical probe was used to collect emission measurements from the combustion products of a methane flame at three equivalence ratios (temperatures). A suction pyrometer was used to collect temperature profiles at the same operating conditions.

- The optical emission measurement contained both gaseous and broadband emissions. A technique was developed to remove the broadband emission from the spectra and calculate the temperature based on only the gaseous emissions.

- The optical measurements produced temperatures approximately 3% higher than the suction pyrometer measurements at the three different conditions.

- The optical pyrometer is estimated to have an uncertainty of ±4% for temperatures at or above 1200 K increasing to nearly 9% at 850 K.

Future work will involve reducing the path length of the measurement volume in order to improve spatial resolution. This can be accomplished by increasing the diameter of the fiber optic cable in order to increase the signal as well as adding a background optical stop to limit the path length. The signal appears strong enough that smaller path lengths could be used with larger fibers, perhaps as low as 5-10 cm. Another area of interest is to use the measurement to determine the relative importance of gaseous and solid particle emission. Once the temperature of the H_2O is known, additional post processing and modeling of the data can be done to determine the H_2O and CO_2 concentrations and total gaseous emissions. This can be compared to the background broadband emission to determine the relative contributions of gas and solids emission. In addition to reducing the path length and improving the spatial resolution, the implementation of band pass filters and detectors can potentially remove the need to use an FTIR with this method, making response times of less than a second possible.

REFERENCES

A. Z'Graggen, H.F., A. Steinfeld. 2007. "Gas temperature measurement in thermal radiating environments using a suction thermocouple apparatus." *Measurement Science and Technology* 18 (11).

A.H.K. Sato, M. Hasatani, S. Sugaiyama, J. Kimura. 1975. "A correctional calculation method for thermocouple measurements of temperatures in flames." *Combustion and Flame* 24: 35-41.

Clausen, S. 1996. "Local measurement of gas temperature with an infrared fibre-optic probe." *Meas. Sci. Technology* 7: 888-896.

D. Backstrom, R. Johansson, K. Anderson, F. Johnsson, S. Clausen, A. Fateev. 2014. "Measurement and modeling of particle radiation in coal flames." *Energy Fuels* 28: 2199-2210.

D. Bradley, K.J.M. 1968. "Measurement of high gas temperature with fine wire thermocouples." *Journal of Mechanical Engineering Science* 10 (4).

Evseev, Vadim, Fateev, Alexander, Clausen. 2012. "High resolution measurements of CO2 at high temperatures for industrial applications." *Journal of Quantitative Spectroscopy and Radiative Transfer* 113 (17): 2222-2233.

F.C. Lockwood, H.A.M. 1982. "Fluctuating temperature measurements in turbulent jet diffusion flame." *Combustion and Flame* 47: 291-314.

Heitor, M.V., Moreira, A.L.N. 1993. "Thermocouples and sample probes for combustion studies." *Combustion Science* p. 259-278.

J.S. Newman, P.A.C. 1979. "Simple aspirated thermocouple for use in fires." *Journal of Fire and Flammability* 10 (4): 326-336.

J.T. Pearson, B.W. Webb, V.P. Solovjov, J. Ma. 2014. "Effect of total pressure on the absorption line blackbody distribution function and radiative transfer in H2O, CO2, and CO." *Journal of the Quantitative Spectroscopy and Radiative Transfer* 143: 100-110.

L.A. Gross, P.R. Griffiths. 1988. "Temperature estimation of carbon dioxide by infrared absorption spectrometry at medium resolution." *Journal of Quantitative Spectroscopy and Radiative Transfer* 39 (2): 131-138.

L.G. Blevins, W.M.P. 1999. "Modeling of bare and aspirated thermocouples in compartment fires." *Fire Safety Journal* 33 (4): 239-259.

L.S. Rothman. I.E.G, R.J. Barber, H. Dothe, R.R. Gamache, A. Goldman, V.I. Perevalov, S.A. Tashkun, J. Tennyson. 2010. "HITEMP, the high temperature molecular spectropic database." *Journal of Quantitative Spectroscopy and Radiative Transfer* 3: 2139-2150.

P.R. Solomon, P.L. Cheien, R.M. Garangelo, P.E. Best, J.R. Markham. 1988. "Application of FTIR emission/transmission spectroscopy to study coal combustion phenomena." *Proceedings of the Combustion Institute.* 211-221.

R. Viskanta, M.P.M. 1987. "Radiation heat transfer in combustion systems." *Progress in Energy and Combustion Science* 13 (2): 97-160.

R.J. Anderson, P.R. Griffiths. 1977. "Determination of rotational temperatures of diatomic molecules from absorption spectra measured at moderate resolution." *Journal of Quantitative Spectroscopy and Radiative Transfer* 17: 393-401.

R.L. Farrow, P.L. Mattern, L.A. Rahn. 1982. "Comparison between CARS and corrected thermocouple temperature measurements in a diffusion flame." *Applied Optics* 21 (17): 3119-3125.

S.C. Kim, A.H. 2008. "On the temperature measurement bias and time response of an aspirated thermocouple in fire environment." *Journal of Fire Sciences* 26 (6).

T. Draper, D. Zeltner, D. Tree, Y. Xue, R. Tsiava. 2012. "Two-dimensional flame temperature and emissivity measurements of pulverized oxy-coal flames." *Applied Energy* 95: 38-44.

T. Ren, T.A. Reeder, M.F. Modest. 2013. "An inverse radiation model for optical determination of temperature and CO2 concentration: development and validation." *International Mechanical Engineering Congress and Exposition.* San Diego, CA.

T.E. Parker, M.F. Miller, K.R. McManus, M.G. Allen, W.T. Rawlins. 1996. "Infrared emission from high-temperature H2O: a diagnostic for concentration and temperature." *AIAA Journal* 34 (3): 500-507.

APPENDIX A.   FTIR SETTINGS

FTIR Settings:

      Source: External

      Type: Transmission Mid IR

      Beam splitter: KBr

      Detector: MCT

      Scans: 32

      Resolution: 0.125

      Data Spacing: 0.060 cm^{-1}

      Range: 5900-3600 cm^{-1}

      Gain: Auto

      Optical Velocity: Auto

      Aperture: Auto

APPENDIX B.   OPTICAL TIME PROGRESSION DATA

Data of optical time progression:

Condition	Test	Epsilon	Planck Temp	E/A	E/B	E/C	Average	St dev	Adiabatic	Time	Time From Start (mins)	TN1	TN2	TN3	TN4
							Without background radiation correction								
1	1			899.54	873.72	864.16	879.14	18.30	1664	1022.00	5.00	306.00	343.00	311.00	296.00
1	2			1101.82	1130.67	1138.91	1123.80	19.48	1664	1025	8.00	326.00	391.00	332.00	296.00
1	3			951.03	937.88	945.60	944.84	6.61	1664	1029	12.00	351.00	439.00	356.00	298.00
1	4			1025.25	1024.65	1022.41	1024.10	1.50	1664	1032	15.00	378.00	482.00	382.00	299.00
1	5			1068.18	1085.90	1095.63	1083.24	13.92	1664	1036	19.00	407.00	521.00	407.00	302.00
1	7			1099.92	1126.79	1130.60	1119.10	16.72	1664	1043	26.00	465.00	589.00	460.00	311.00
1	8			1160.31	1203.79	1215.08	1193.06	28.92	1664	1047	30.00	490.00	615.00	481.00	315.00
1	9			1149.71	1190.09	1204.08	1181.29	28.23	1664	1050	33.00	513.00	640.00	502.00	321.00
1	10			1098.41	1115.63	1120.88	1111.64	11.75	1664	1053	36.00	535.00	665.00	523.00	328.00
1	11			1173.99	1211.79	1215.02	1200.27	22.81	1664	1057	40.00	554.00	684.00	540.00	333.00
1	12			1199.99	1250.49	1260.39	1236.96	32.39	1664	1100	43.00	572.00	702.00	557.00	340.00
1	13			1173.50	1215.54	1227.89	1205.64	28.51	1664	1104	47.00	590.00	719.00	573.00	348.00
1	14			1172.99	1218.56	1231.59	1207.71	30.77	1664	1108	51.00	609.00	736.00	590.00	356.00
1	15			1288.13	1338.29	1338.42	1321.61	29.00	1664	1111	54.00	624.00	750.00	603.00	363.00
1	16			1278.47	1331.48	1345.02	1318.32	35.17	1664	1114	57.00	639.00	763.00	616.00	371.00
1	17			1297.64	1353.13	1355.17	1335.31	32.64	1664	1122	65.00	675.00	795.00	647.00	390.00
1	18			1274.11	1323.03	1332.05	1309.73	31.18	1664	1134	77.00	720.00	833.00	685.00	415.00
1	19			1314.77	1371.74	1380.15	1355.55	35.57	1664	1137	80.00	732.00	843.00	695.00	424.00
1	20			1379.00	1409.00	1427.32	1405.11	24.39	1664	1141	84.00	744.00	853.00	706.00	432.00
1	21			1340.13	1398.80	1399.37	1379.43	34.04	1664	1144	87.00	759.00	865.00	718.00	442.00
1	22			1330.77	1391.47	1395.63	1372.62	36.30	1664	1148	91.00	769.00	874.00	727.00	449.00
1	23			1364.21	1430.23	1427.90	1407.45	37.46	1664	1155	98.00	793.00	892.00	747.00	466.00
1	24			1333.18	1397.85	1403.37	1378.13	39.03	1664	1201	104.00	809.00	904.00	761.00	479.00
1	25			1465.27	1528.88	1523.95	1506.03	35.39	1664	1212	115.00	838.00	927.00	786.00	503.00
1	26			1453.19	1527.08	1523.47	1501.24	41.66	1664	1217	120.00	852.00	937.00	799.00	515.00
1	27			1434.59	1506.07	1505.42	1482.03	41.08	1664	1229	132.00	879.00	958.00	823.00	539.00
1	28			1471.48	1551.71	1556.21	1526.47	47.67	1664	1240	143.00	900.00	974.00	841.00	557.00
1	31			1521.74	1629.22	1615.10	1588.69	58.40	1664	109	172.00	949.00	1011.00	885.00	604.00
1	32			1545.83	1655.16	1639.48	1613.49	59.12	1664	120	183.00	966.00	1024.00	901.00	620.00
1	33			1551.21	1647.62	1630.44	1609.76	51.42	1664	130	193.00	977.00	1031.00	910.00	631.00
1	34			1604.60	1719.43	1691.46	1671.83	59.88	1664	140	203.00	987.00	1040.00	921.00	642.00
1	35			1612.89	1732.50	1718.38	1687.93	65.37	1664	150	213.00	998.00	1048.00	931.00	653.00
1	36			1645.17	1778.74	1754.00	1725.97	71.06	1664	200	223.00	1008.00	1056.00	940.00	663.00
1	37			1631.02	1778.99	1757.03	1722.35	79.85	1664	214	237.00	1018.00	1063.00	951.00	675.00

Condition	Test	Epsilon	Planck Temp	E/A	E/B	E/C	Average	St dev	Adiabatic	Time	Time From Start (mins)	TN1	TN2	TN3	TN4
1	1	0.027268	700.65	747.26	706.18	686.80	713.41	30.88	1664	1022.00	5.00	306.00	343.00	311.00	296.00
1	2	0.2	600.00	1069.79	1081.54	1086.23	1079.19	8.47	1664	1025	8.00	326.00	391.00	332.00	296.00
1	3	0.02078	749.23	824.07	789.28	786.47	799.94	20.94	1664	1029	12.00	351.00	439.00	356.00	298.00
1	4	0.015224	805.03	882.88	843.29	827.87	851.35	28.37	1664	1032	15.00	378.00	482.00	382.00	299.00
1	5	0.020767	774.57	1001.98	990.70	993.21	995.30	5.92	1664	1036	19.00	407.00	521.00	407.00	302.00
1	7	0.069856	710.85	1030.60	1023.83	1020.08	1024.84	5.33	1664	1043	26.00	465.00	589.00	460.00	311.00
1	8	0.011362	909.52	1024.63	1011.04	1011.91	1015.86	7.60	1664	1047	30.00	490.00	615.00	481.00	315.00
1	9	0.210859	655.08	1090.01	1103.02	1112.32	1101.79	11.21	1664	1050	33.00	513.00	640.00	502.00	321.00
1	10	0.038067	783.47	987.30	955.61	948.80	963.90	20.55	1664	1053	36.00	535.00	665.00	523.00	328.00
1	11	0.092867	726.31	1084.30	1086.53	1085.14	1085.33	1.13	1664	1057	40.00	554.00	684.00	540.00	333.00
1	12	0.073938	755.41	1088.60	1097.20	1102.58	1096.13	7.05	1664	1100	43.00	572.00	702.00	557.00	340.00
1	13	0.209375	679.69	1083.70	1087.98	1094.33	1088.67	5.34	1664	1104	47.00	590.00	719.00	573.00	348.00
1	14	0.2125	680.00	1086.04	1094.50	1101.86	1094.13	7.92	1664	1108	51.00	609.00	736.00	590.00	356.00
1	15	0.079731	761.00	1156.73	1175.55	1179.67	1170.65	12.23	1664	1111	54.00	624.00	750.00	603.00	363.00
1	16	0.07883	777.68	1147.98	1168.08	1181.17	1165.74	16.72	1664	1114	57.00	639.00	763.00	616.00	371.00
1	17	0.108943	762.98	1154.58	1174.63	1180.60	1169.93	13.63	1664	1122	65.00	675.00	795.00	647.00	390.00
1	18	0.055239	840.99	1087.39	1084.09	1089.79	1087.09	2.86	1664	1134	77.00	720.00	833.00	685.00	415.00
1	19	0.04679	861.45	1117.26	1126.23	1135.55	1126.35	9.14	1664	1137	80.00	732.00	843.00	695.00	424.00
1	20	0.038908	889.30	1133.20	1135.39	1151.85	1140.14	10.19	1664	1141	84.00	744.00	853.00	706.00	432.00
1	21	0.092279	803.61	1143.39	1156.72	1163.19	1154.43	10.09	1664	1144	87.00	759.00	865.00	718.00	442.00
1	22	0.085343	811.49	1138.20	1152.67	1160.93	1150.60	11.51	1664	1148	91.00	769.00	874.00	727.00	449.00
1	23	0.2	750.00	1182.77	1204.26	1210.60	1199.21	14.59	1664	1155	98.00	793.00	892.00	747.00	466.00
1	24	0.206875	748.13	1152.49	1170.62	1179.96	1167.69	13.97	1664	1201	104.00	809.00	904.00	761.00	479.00
1	25	0.114043	811.00	1223.45	1235.04	1244.11	1234.20	10.36	1664	1212	115.00	838.00	927.00	786.00	503.00
1	26	0.091416	836.06	1186.38	1201.00	1210.92	1199.43	12.34	1664	1217	120.00	852.00	937.00	799.00	515.00
1	27	0.112344	821.02	1179.46	1194.07	1204.58	1192.70	12.62	1664	1229	132.00	879.00	958.00	823.00	539.00
1	28	0.073484	877.60	1162.71	1174.24	1188.68	1175.21	13.01	1664	1240	143.00	900.00	974.00	841.00	557.00
1	31	0.083466	880.23	1172.66	1189.06	1197.72	1186.48	12.73	1664	109	172.00	949.00	1011.00	885.00	604.00
1	32	0.08197	888.66	1181.09	1195.86	1204.88	1193.95	12.01	1664	120	183.00	966.00	1024.00	901.00	620.00
1	33	0.083646	887.71	1184.43	1193.46	1201.52	1193.14	8.55	1664	130	193.00	977.00	1031.00	910.00	631.00
1	34	0.103868	869.00	1234.35	1245.37	1250.51	1243.41	8.26	1664	140	203.00	987.00	1040.00	921.00	642.00
1	35	0.116037	860.65	1263.08	1276.68	1288.29	1276.02	12.62	1664	150	213.00	998.00	1048.00	931.00	653.00
1	36	0.06558	932.39	1214.33	1226.78	1236.72	1225.94	11.21	1664	200	223.00	1008.00	1056.00	940.00	663.00
1	37	0.08231	908.01	1219.51	1239.93	1250.70	1236.72	15.84	1664	214	237.00	1018.00	1063.00	951.00	675.00

Condition	Test	Cv Temp	Epsilon	Planck Temp	E/A	E/B	E/C	Average	St dev	Adiabatic	Time	Time From Start (mins)	TN1	TN2	TN3	TN4
2	1	1223			1062.00	1084.08	1106.89	1084.32	22.45	1862	11:16	6	306	348	312	295
2										1862	11:18	8	318	377	325	295
2	2	1223			1.08E+03	1.10E+03	1.11E+03			1862	11:21	11	338	420	345	296
2										1862	11:23	13	353	450	360	296
2										1862	11:25	15	377	486	383	298
2	3	1223			1.13E+03	1.17E+03	1.17E+03			1862	11:26	16	385	498	391	298
2										1862	11:28	18	400	520	405	299
2	4	1223			1.15E+03	1.19E+03	1.19E+03			1862	11:30	20	421	549	425	301
2										1862	11:32	22	442	576	444	304
2										1862	11:34	24	454	594	456	306
2	5	1223			1.17E+03	1.21E+03	1.22E+03			1862	11:35	25	465	608	466	307
2										1862	11:37	27	481	628	481	310
2	6	1223			1.22E+03	1.26E+03	1.27E+03			1862	11:39	29	497	648	497	313
2										1862	11:41	31	512	666	510	316
2										1862	11:43	33	529	685	526	320
2	7	1223			1.24E+03	1.28E+03	1.29E+03			1862	11:44	34	540	697	536	323
2										1862	11:46	36	553	711	547	326
2	8	1223			1.27E+03	1.32E+03	1.32E+03			1862	11:48	38	566	724	559	330
2										1862	11:50	40	580	738	572	334
2										1862	11:52	42	594	751	585	338
2	9	1223			1.31E+03	1.36E+03	1.36E+03			1862	11:54	44	607	763	597	343
2										1862	11:56	46	624	779	612	350
2	10	1223			1.37E+03	1.43E+03	1.44E+03			1862	11:58	48	634	790	622	354
2										1862	12:00	50	644	797	629	357
2	11	1223			1.33E+03	1.39E+03	1.38E+03			1862	12:02	52	658	810	641	363
2										1862	12:04	54	668	818	649	367
2	12	1223			1.35E+03	1.40E+03	1.40E+03			1862	12:06	56	682	830	662	374
2										1862	12:08	58	690	836	668	378
2										1862	12:10	60	699	844	676	382
2	13	1223			1.39E+03	1.45E+03	1.45E+03			1862	12:12	62	709	852	685	388
2										1862	12:14	64	719	860	692	393
2										1862	12:16	66	728	868	700	398
2	14	1223			1.46E+03	1.52E+03	1.51E+03			1862	12:20	70	748	883	716	409
2										1862	12:22	72	756	890	724	414
2										1862	12:24	74	766	898	732	420
2	15	1223			1.46E+03	1.52E+03	1.52E+03			1862	12:26	76	775	905	739	426
2										1862	12:28	78	783	911	745	431
2	16	1223			1.48E+03	1.54E+03	1.53E+03			1862	12:30	80	791	917	753	437
2										1862	12:32	82	800	924	759	442
2										1862	12:34	84	807	929	765	447
2	17	1223			1.53E+03	1.61E+03	1.60E+03			1862	12:36	86	817	937	773	454
2										1862	12:38	88	825	943	780	460
2										1862	12:40	90	830	947	785	464
2	18	1223			1.52E+03	1.60E+03	1.59E+03			1862	12:42	92	838	954	792	470
2										1862	12:44	94	844	958	796	475
2										1862	12:46	96	850	963	802	480
2	19	1223			1.55E+03	1.64E+03	1.62E+03			1862	12:48	98	857	968	808	486
2										1862	12:50	100	864	974	814	491
2	20	1223			1.56E+03	1.63E+03	1.62E+03			1862	12:52	102	871	978	819	497
2										1862	12:54	104	877	983	825	502
2										1862	12:56	106	884	987	830	507
2	21	1223			1.56E+03	1.65E+03	1.64E+03			1862	12:58	108	889	992	835	512
2										1862	1:00	110	895	996	840	517
2	22	1223			1.60E+03	1.68E+03	1.67E+03			1862	1:02	112	902	1001	846	522
2										1862	1:04	114	906	1004	849	526
2										1862	1:06	116	912	1010	855	533
2	23	1223			1.60E+03	1.69E+03	1.68E+03			1862	1:08	118	916	1013	858	535
2										1862	1:10	120	922	1017	863	540
2	24	1223			1.61E+03	1.71E+03	1.70E+03			1862	1:15	125	935	1026	874	552
2	25	1223			1.63E+03	1.74E+03	1.72E+03			1862	1:22	132	952	1039	890	567
2	26	1223			1.66E+03	1.78E+03	1.75E+03			1862	1:30	140	970	1052	905	584
2	27	1223			1.67E+03	1.79E+03	1.76E+03			1862	1:37	147	983	1062	917	597
2	28	1223			1.68E+03	1.80E+03	1.77E+03			1862	1:44	154	997	1071	930	611
2	29	1223			1.69E+03	1.83E+03	1.79E+03			1862	1:52	162	1011	1082	942	624
2	30	1223			1.71E+03	1.85E+03	1.81E+03			1862	2:01	171	1025	1093	955	639
2	31	1223			1.72E+03	1.85E+03	1.82E+03			1862	2:08	178	1036	1100	966	649
2	32	1223			1.73E+03	1.86E+03	1.83E+03			1862	2:15	185	1046	1107	974	659
2	33	1223			1.73E+03	1.86E+03	1.83E+03			1862	2:23	193	1056	1114	983	670
2	34	1223			1.74E+03	1.89E+03	1.86E+03			1862	2:31	201	1065	1122	993	679
2										1862	2:44	214	1079	1132	1006	693
2										1862	2:48	218	1083	1135	1010	698
2	35	1223			1.81E+03	1.96E+03	1.93E+03			1862	3:21	251	1110	1155	1037	727
2	36	1223			1.86E+03	2.02E+03	1.98E+03			1862	3:31	261	1116	1160	1043	734

Condition	Test	Cv Temp	Epsilon	Planck Temp	E/A	E/B	E/C	Average	St dev	Adiabatic	Time	Time From Start (mins)	TN1	TN2	TN3	TN4
						With background radiation correction											
2	1	1223	1.132522	511.9610016	1045.15	1057.75	1078.25	1060.38	16.71	1862	11:16	6	306	348	312	295
2										1862	11:18	8	318	377	325	295
2	2	1223	0.200395	643.328403	1.04E+03	1.04E+03	1.04E+03	1042.20		1862	11:21	11	338	420	345	296
2										1862	11:23	13	353	450	360	296
2										1862	11:25	15	377	486	383	298
2	3	1223	1.14317	564.366703	1.10E+03	1.13E+03	1.13E+03	1121.24		1862	11:26	16	385	498	391	298
2										1862	11:28	18	400	520	405	299
2	4	1223	0.033061	817.4419289	1.08E+03	1.09E+03	1.09E+03	1083.73		1862	11:30	20	421	549	425	301
2										1862	11:32	22	442	576	444	304
2										1862	11:34	24	454	594	456	306
2	5	1223	0.041947	826.817177	1.08E+03	1.08E+03	1.08E+03	1078.85		1862	11:35	25	465	608	466	307
2										1862	11:37	27	481	628	481	310
2	6	1223	0.545976	642.5039237	1.16E+03	1.18E+03	1.19E+03	1177.50		1862	11:39	29	497	648	497	313
2										1862	11:41	31	512	666	510	316
2										1862	11:43	33	529	685	526	320
2	7	1223	0.0613	826.6493974	1.11E+03	1.12E+03	1.13E+03	1123.27		1862	11:44	34	540	697	536	323
2										1862	11:46	36	553	711	547	326
2	8	1223	0.205	731.25	1.16E+03	1.19E+03	1.19E+03	1180.55		1862	11:48	38	566	724	559	330
2										1862	11:50	40	580	738	572	334
2										1862	11:52	42	594	751	585	338
2	9	1223	0.061698	853.1455321	1.15E+03	1.17E+03	1.18E+03	1168.76		1862	11:54	44	607	763	597	343
2										1862	11:56	46	624	779	612	350
2	10	1223	0.064513	866.8173995	1.18E+03	1.20E+03	1.21E+03	1199.30		1862	11:58	48	634	790	622	354
2										1862	12:00	50	644	797	629	357
2	11	1223	0.05787	888.1813826	1.13E+03	1.14E+03	1.14E+03	1135.40		1862	12:02	52	658	810	641	363
2										1862	12:04	54	668	818	649	367
2	12	1223	0.142035	804.4015094	1.17E+03	1.18E+03	1.19E+03	1180.16		1862	12:06	56	682	830	662	374
2										1862	12:08	58	690	836	668	378
2										1862	12:10	60	699	844	676	382
2	13	1223	0.090546	862.8161776	1.17E+03	1.18E+03	1.19E+03	1182.31		1862	12:12	62	709	852	685	388
2										1862	12:14	64	719	860	692	393
2										1862	12:16	66	728	868	700	398
2	14	1223	0.065243	911.3762075	1.19E+03	1.21E+03	1.22E+03	1205.60		1862	12:20	70	748	883	716	409
2										1862	12:22	72	756	890	724	414
2										1862	12:24	74	766	898	732	420
2	15	1223	0.077376	901.9450375	1.18E+03	1.20E+03	1.21E+03	1195.60		1862	12:26	76	775	905	739	426
2										1862	12:28	78	783	911	745	431
2	16	1223	0.087989	890.8336339	1.21E+03	1.22E+03	1.23E+03	1216.94		1862	12:30	80	791	917	753	437
2										1862	12:32	82	800	924	759	442
2										1862	12:34	84	807	929	765	447
2	17	1223	0.078355	913.9796415	1.23E+03	1.24E+03	1.25E+03	1240.37		1862	12:36	86	817	937	773	454
2										1862	12:38	88	825	943	780	460
2										1862	12:40	90	830	947	785	464
2	18	1223	0.069	938.4827163	1.19E+03	1.21E+03	1.22E+03	1205.25		1862	12:42	92	838	954	792	470
2										1862	12:44	94	844	958	796	475
2										1862	12:46	96	850	963	802	480
2	19	1223	0.077269	931.9389129	1.23E+03	1.24E+03	1.25E+03	1240.03		1862	12:48	98	857	968	808	486
2										1862	12:50	100	864	974	814	491
2	20	1223	0.093082	914.7964767	1.22E+03	1.22E+03	1.23E+03	1224.46		1862	12:52	102	871	978	819	497
2										1862	12:54	104	877	983	825	502
2										1862	12:56	106	884	987	830	507
2	21	1223	0.210859	829.765625	1.28E+03	1.29E+03	1.30E+03	1289.57		1862	12:58	108	889	992	835	512
2										1862	1:00	110	895	996	840	517
2	22	1223	0.119794	894.7892596	1.27E+03	1.28E+03	1.29E+03	1280.54		1862	1:02	112	902	1001	846	522
2										1862	1:04	114	906	1004	849	526
2										1862	1:06	116	912	1010	855	533
2	23	1223	0.105484	913.5719267	1.25E+03	1.26E+03	1.27E+03	1261.61		1862	1:08	118	916	1013	858	535
2										1862	1:10	120	922	1017	863	540
2	24	1223	0.089842	943.065638	1.22E+03	1.23E+03	1.24E+03	1231.59		1862	1:15	125	935	1026	874	552
2	25	1223	0.2125	850	1.29E+03	1.29E+03	1.30E+03	1293.76		1862	1:22	132	952	1039	890	567
2	26	1223	0.089502	951.8707875	1.24E+03	1.25E+03	1.26E+03	1252.56		1862	1:30	140	970	1052	905	584
2	27	1223	0.091955	953.2740387	1.26E+03	1.26E+03	1.27E+03	1263.19		1862	1:37	147	983	1062	917	597
2	28	1223	0.094332	955.8257801	1.26E+03	1.26E+03	1.27E+03	1265.70		1862	1:44	154	997	1071	930	611
2	29	1223	0.211406	865.625	1.32E+03	1.33E+03	1.33E+03	1327.87		1862	1:52	162	1011	1082	942	624
2	30	1223	0.100582	952.8514777	1.27E+03	1.28E+03	1.28E+03	1276.33		1862	2:01	171	1025	1093	955	639
2	31	1223	0.095671	963.6872683	1.28E+03	1.28E+03	1.29E+03	1279.53		1862	2:08	178	1036	1100	966	649
2	32	1223	0.089933	975.2898958	1.27E+03	1.27E+03	1.28E+03	1272.70		1862	2:15	185	1046	1107	974	659
2	33	1223	0.11641	947.2118427	1.27E+03	1.28E+03	1.29E+03	1278.39		1862	2:23	193	1056	1114	983	670
2	34	1223	0.092353	983.9022282	1.26E+03	1.26E+03	1.27E+03	1265.52		1862	2:31	201	1065	1122	993	679
2										1862	2:44	214	1079	1132	1006	693
2										1862	2:48	218	1083	1135	1010	698
2	35	1223	0.093109	969.2962958	1.30E+03	1.30E+03	1.31E+03	1303.09		1862	3:21	251	1110	1155	1037	727
2	36	1223	0.086665	981.9772648	1.32E+03	1.32E+03	1.33E+03	1323.02		1862	3:31	261	1116	1160	1043	734

											Without background radiation correction					
Condition	Test	Cv Temp	Epsilon	Planck Temp	E/A	E/B	E/C	Average	St dev	Adiabatic	Time	Time From Start (mins)	TN1	TN2	TN3	TN4
3	1	1223			1130.15	1158.56	1181.00	1156.57	25.48	2024	11:24	5	300	338	309	295
3										2024	11:30	11	334	434	354	296
3	2	1223			1190.77	1225.34	1239.79	1218.63	25.19	2024	11:31	12	343	452	364	297
3										2024	11:33	15	362	487	385	298
3										2024	11:36	18	395	540	420	300
3	3	1223			1223.63	1260.63	1275.81	1253.35	26.84	2024	11:38	20	409	561	435	302
3										2024	11:40	22	434	594	458	305
3	4	1223			1237.07	1273.48	1285.36	1265.30	25.16	2024	11:41	23	445	608	468	306
3										2024	11:43	25	464	631	485	309
3	5	1223			1275.12	1310.42	1325.49	1303.68	25.85	2024	11:45	27	479	650	499	312
3										2024	11:47	29	497	672	516	315
3	6	1223			1303.53	1340.44	1353.00	1332.33	25.71	2024	11:48	30	513	689	530	318
3										2024	11:50	32	528	707	543	322
3	7	1223			1315.97	1353.95	1364.01	1344.64	25.34	2024	11:52	34	548	728	561	326
3										2024	11:54	36	558	739	571	329
3										2024	11:56	38	574	755	585	334
3										2024	11:58	40	590	770	598	338
3	8	1223			1364.90	1409.44	1420.01	1398.12	29.25	2024	12:00	42	607	786	613	344
3										2024	12:02	44	620	798	625	349
3	9	1223			1389.37	1428.47	1434.21	1417.35	24.40	2024	12:04	46	635	812	637	354
3										2024	12:06	48	648	825	650	360
3										2024	12:08	50	664	837	662	366
3	10	1223			1422.53	1461.01	1467.21	1450.25	24.21	2024	12:10	52	677	849	674	371
3										2024	12:12	54	692	863	687	378
3	11	1223			1427.91	1471.79	1473.96	1457.88	25.98	2024	12:14	56	706	873	698	384
3										2024	12:16	58	713	880	703	388
3										2024	12:18	60	727	891	715	395
3	12	1223			1482.61	1533.66	1532.14	1516.14	29.05	2024	12:20	62	738	900	725	401
3										2024	12:22	64	748	908	733	407
3	13	1223			1484.30	1532.82	1533.13	1516.75	28.10	2024	12:24	66	761	918	744	414
3										2024	12:26	68	774	929	755	421
3										2024	12:28	70	786	939	764	429
3	14	1223			1518.49	1574.42	1572.37	1555.09	31.72	2024	12:30	72	792	943	770	432
3										2024	12:32	74	800	950	777	438
3	15	1223			1534.56	1594.71	1589.23	1572.83	33.26	2024	12:34	76	812	959	786	446
3										2024	12:36	78	819	965	792	450
3										2024	12:38	80	828	972	800	457
3	16	1223			1552.91	1617.58	1608.21	1592.90	34.95	2024	12:40	82	837	979	808	463
3										2024	12:42	84	847	987	817	470
3	17	1223			1563.54	1632.14	1625.13	1606.94	37.75	2024	12:44	86	855	993	823	476
3										2024	12:46	88	864	999	831	482
3										2024	12:48	90	873	1006	838	489
3	18	1223			1631.06	1718.25	1706.62	1685.31	47.34	2024	12:50	92	879	1011	843	494
3										2024	12:52	94	888	1017	850	501
3										2024	12:54	96	895	1023	856	507
3	19	1223			1644.01	1726.88	1709.97	1693.62	43.79	2024	12:56	98	901	1027	861	511
3										2024	12:58	100	909	1033	868	519
3	20	1223			1646.03	1740.77	1722.49	1703.10	50.26	2024	1:00	102	915	1038	873	523
3										2024	1:02	104	923	1043	879	529
3										2024	1:04	106	930	1049	886	535
3	21	1223			1644.95	1732.69	1716.33	1697.99	46.66	2024	1:06	108	935	1052	890	540
3										2024	1:08	110	943	1058	896	547
3	22	1223			1651.33	1739.63	1722.54	1704.50	46.83	2024	1:10	112	949	1063	902	552
3										2024	1:12	114	954	1066	906	556
3										2024	1:14	116	961	1071	911	562
3	23	1223			1681.77	1772.75	1754.35	1736.29	48.10	2024	1:16	118	967	1075	916	567
3										2024	1:18	120	972	1079	921	572
3	24	1223			1706.93	1811.28	1788.26	1768.82	54.82	2024	1:22	124	983	1087	930	582
3	25	1223			1702.43	1809.55	1786.11	1766.03	56.31	2024	1:26	128	994	1095	940	592
3	26	1223			1737.32	1848.77	1824.95	1803.68	58.69	2024	1:32	134	1009	1106	953	606
3	27	1223			1727.15	1837.21	1813.68	1792.68	57.96	2024	1:36	138	1018	1112	961	614
3	28	1223			1751.64	1865.95	1843.57	1820.39	60.58	2024	1:42	144	1032	1123	973	627
3	29	1223			1744.04	1858.63	1831.96	1811.54	59.96	2024	1:48	150	1046	1132	985	641
3	30	1223			1751.02	1873.44	1845.93	1823.46	64.22	2024	1:52	154	1053	1137	991	647
3	31	1223			1818.20	1908.75	1850.76	1859.24	45.87	2024	2:00	162	1068	1148	1005	662
3	32	1223			1793.24	1916.58	1885.25	1865.02	64.11	2024	2:06	168	1079	1156	1015	673
3	33	1223			1810.04	1937.66	1905.97	1884.56	66.45	2024	2:10	172	1085	1161	1021	679
3	34	1223			1805.41	1939.77	1899.97	1881.71	69.02	2024	2:16	178	1095	1168	1029	689
3	35	1223			1819.55	1952.06	1913.29	1894.96	68.13	2024	2:20	182	1102	1172	1035	695
3	36	1223			1824.19	1953.74	1913.54	1897.15	66.31	2024	2:26	188	1111	1180	1044	705
3	37	1223			1837.71	1966.14	1931.24	1911.69	66.41	2024	2:30	192	1116	1183	1048	709
3	38	1223			1838.73	1965.58	1932.01	1912.11	65.73	2024	2:36	198	1123	1188	1055	717
3	39	1223			1846.99	1974.48	1936.87	1919.45	65.51	2024	2:40	202	1128	1192	1059	722
3	40	1223			1853.72	1982.77	1944.27	1926.92	66.25	2024	2:50	212	1138	1200	1069	734
3	41	1223			1868.13	2004.87	1962.26	1945.09	69.97	2024	3:00	222	1148	1208	1079	744
3	42	1223			1865.61	1996.54	1962.09	1941.42	67.87	2024	3:10	232	1158	1215	1089	754
3	43	1223			1892.41	2026.04	1983.86	1967.44	68.31	2024	3:20	242	1166	1221	1097	762
3	44	1223			1912.39	2044.42	1999.99	1985.60	67.18	2024	3:30	252	1174	1227	1104	770
3	46	1223			1917.48	2058.57	2012.07	1996.04	71.90	2024	3:55	277	1190	1240	1117.95	788.75

With background radiation correction

Condition	Test	Cv Temp	Epsilon	Planck Temp	E/A	E/B	E/C	Average	St dev	Adiabatic	Time	Time From Start (mins)	TN1	TN2	TN3	TN4
3	1	1223	0.029574	777.45	1084.64	1093.13	1111.30	1096.35	13.62	2024	11:24	5	300	338	309	295
3										2024	11:30	11	334	434	354	296
3	2	1223	0.215625	662.50	1152.95	1175.51	1188.54	1172.33	18.01	2024	11:31	12	343	452	364	297
3										2024	11:33	15	362	487	385	298
3										2024	11:36	18	395	540	420	300
3	3	1223	0.035884	835.69	1142.47	1159.59	1173.00	1158.35	15.30	2024	11:38	20	409	561	435	302
3										2024	11:40	22	434	594	458	305
3	4	1223	0.084916	773.41	1160.50	1179.28	1190.61	1176.80	15.21	2024	11:41	23	445	608	468	306
3										2024	11:43	25	464	631	485	309
3	5	1223	0.074146	798.73	1177.09	1193.96	1208.77	1193.27	15.85	2024	11:45	27	479	650	499	312
3										2024	11:47	29	497	672	516	315
3	6	1223	0.209961	726.60	1213.62	1232.78	1246.49	1230.96	16.51	2024	11:48	30	513	689	530	318
3										2024	11:50	32	528	707	543	322
3	7	1223	0.063946	847.49	1180.76	1195.99	1208.37	1195.04	13.83	2024	11:52	34	548	728	561	326
3										2024	11:54	36	558	739	571	329
3										2024	11:56	38	574	755	585	334
3										2024	11:58	40	590	770	598	338
3	8	1223	0.097981	822.62	1215.63	1233.51	1248.07	1232.40	16.25	2024	12:00	42	607	786	613	344
3										2024	12:02	44	620	798	625	349
3	9	1223	0.053603	906.59	1192.99	1203.38	1215.69	1204.02	11.37	2024	12:04	46	635	812	637	354
3										2024	12:06	48	648	825	650	360
3										2024	12:08	50	664	837	662	366
3	10	1223	0.067619	889.74	1216.65	1224.69	1238.45	1226.60	11.03	2024	12:10	52	677	849	674	371
3										2024	12:12	54	692	863	687	378
3	11	1223	0.082249	880.37	1209.17	1218.20	1229.87	1219.08	10.38	2024	12:14	56	706	873	698	384
3										2024	12:16	58	713	880	703	388
3										2024	12:18	60	727	891	715	395
3	12	1223	0.08117	893.25	1252.39	1261.07	1272.70	1262.05	10.19	2024	12:20	62	738	900	725	401
3										2024	12:22	64	748	908	733	407
3	13	1223	0.2125	807.50	1270.81	1274.96	1286.65	1277.47	8.21	2024	12:24	66	761	918	744	414
3										2024	12:26	68	774	929	755	421
3										2024	12:28	70	786	939	764	429
3	14	1223	0.082416	912.68	1252.72	1258.13	1271.18	1260.68	9.49	2024	12:30	72	792	943	770	432
3										2024	12:32	74	800	950	777	438
3	15	1223	0.127829	870.12	1281.14	1285.38	1296.37	1287.63	7.86	2024	12:34	76	812	959	786	446
3										2024	12:36	78	819	965	792	450
3										2024	12:38	80	828	972	800	457
3	16	1223	0.087628	920.26	1257.65	1261.44	1272.16	1263.75	7.53	2024	12:40	82	837	979	808	463
3										2024	12:42	84	847	987	817	470
3	17	1223	0.092101	921.41	1261.72	1265.61	1278.08	1268.47	8.55	2024	12:44	86	855	993	823	476
3										2024	12:46	88	864	999	831	482
3										2024	12:48	90	873	1006	838	489
3	18	1223	0.2	850.00	1350.42	1349.28	1359.37	1353.02	5.53	2024	12:50	92	879	1011	843	494
3										2024	12:52	94	888	1017	850	501
3										2024	12:54	96	895	1023	856	507
3	19	1223	0.09401	934.98	1321.64	1318.78	1328.39	1322.94	4.94	2024	12:56	98	901	1027	861	511
3										2024	12:58	100	909	1033	868	519
3	20	1223	0.2125	850.00	1361.53	1361.59	1368.04	1363.72	3.74	2024	1:00	102	915	1038	873	523
3										2024	1:02	104	923	1043	879	529
3										2024	1:04	106	930	1049	886	535
3	21	1223	0.090663	951.74	1294.68	1293.77	1304.95	1297.80	6.21	2024	1:06	108	935	1052	890	540
3										2024	1:08	110	943	1058	896	547
3	22	1223	0.098996	947.27	1296.14	1293.82	1304.85	1298.27	5.82	2024	1:10	112	949	1063	902	552
3										2024	1:12	114	954	1066	906	556
3										2024	1:14	116	961	1071	911	562
3	23	1223	0.100527	948.24	1318.62	1311.66	1322.86	1317.71	5.66	2024	1:16	118	967	1075	916	567
3										2024	1:18	120	972	1079	921	572
3	24	1223	0.10149	948.92	1341.08	1336.45	1345.91	1341.15	4.73	2024	1:22	124	983	1087	930	582
3	25	1223	0.120274	930.45	1340.13	1336.54	1345.44	1340.70	4.48	2024	1:26	128	994	1095	940	592
3	26	1223	0.094738	967.57	1349.00	1343.00	1353.79	1348.60	5.41	2024	1:32	134	1009	1106	953	606
3	27	1223	0.088105	983.11	1311.79	1306.58	1318.48	1312.28	5.97	2024	1:36	138	1018	1112	961	614
3	28	1223	0.228672	871.17	1415.70	1404.58	1412.82	1411.03	5.77	2024	1:42	144	1032	1123	973	627
3	29	1223	0.103447	969.70	1325.88	1318.94	1329.58	1324.80	5.40	2024	1:48	150	1046	1132	985	641
3	30	1223	0.125316	944.79	1359.62	1355.23	1364.29	1359.71	4.53	2024	1:52	154	1053	1137	991	647
3	32	1223	0.2125	892.50	1424.09	1411.17	1416.47	1417.24	6.50	2024	2:06	168	1079	1156	1015	673
3	33	1223	0.117962	965.77	1373.21	1362.17	1372.19	1369.19	6.10	2024	2:10	172	1085	1161	1021	679
3	34	1223	0.105006	982.30	1345.69	1338.87	1345.80	1343.45	3.97	2024	2:16	178	1095	1168	1029	689
3	35	1223	0.107317	981.02	1358.62	1349.00	1356.64	1354.75	5.08	2024	2:20	182	1102	1172	1035	695
3	36	1223	0.101135	992.91	1353.77	1342.68	1350.12	1348.86	5.65	2024	2:26	188	1111	1180	1044	705
3	37	1223	0.099125	996.03	1361.14	1348.03	1358.86	1356.01	7.01	2024	2:30	192	1116	1183	1048	709
3	38	1223	0.199355	912.48	1430.38	1412.82	1419.81	1420.99	8.86	2024	2:36	198	1123	1188	1055	717
3	39	1223	0.199355	912.48	1435.70	1417.54	1422.29	1425.18	9.42	2024	2:40	202	1128	1192	1059	722
3	40	1223	0.111704	987.12	1371.15	1355.65	1364.94	1363.92	7.80	2024	2:50	212	1138	1200	1069	734
3	41	1223	0.099347	1011.90	1350.42	1338.41	1347.85	1345.56	6.33	2024	3:00	222	1148	1208	1079	744
3	42	1223	0.100689	1009.70	1351.44	1336.65	1350.05	1346.05	8.17	2024	3:10	232	1158	1215	1089	754
3	43	1223	0.107478	1005.53	1378.32	1362.69	1372.42	1371.15	7.89	2024	3:20	242	1166	1221	1097	762
3	44	1223	0.119438	993.28	1400.85	1382.45	1390.87	1391.39	9.21	2024	3:30	252	1174	1227	1104	770
3	46	1223	0.114606	1004.34	1382.15	1368.04	1377.08	1375.75	7.15	2024	3:55	277	1190	1240	1117.95	788.75